arXiv:1301.3742v1 [astro-ph.EP] 16 Jan 2013

Response of the Jovian thermosphere to a transient 'pulse' in solar wind pressure

J. N. Yates[a,b,*], N. Achilleos[a,b], P. Guio[a,b]

[a] *Department of Physics and Astronomy, University College London, Gower Street, London, UK*
[b] *Centre for Planetary Sciences at UCL / Birkbeck, University College London, Gower Street, London, UK*

Abstract

The importance of the Jovian thermosphere with regard to magnetosphere-ionosphere coupling is often neglected in magnetospheric physics. We present the first study to investigate the response of the Jovian thermosphere to transient variations in solar wind dynamic pressure, using an azimuthally symmetric global circulation model coupled with a simple magnetosphere model. In our simulations, the Jovian magnetosphere encounters a solar wind shock or rarefaction region and is subsequently compressed or expanded. We present the ensuing response of the thermospheric flows, momentum sources, and the coupling currents, to these transient events. Transient compressions cause the reversal of magnetosphere-ionosphere coupling currents and momentum transfer between the thermosphere and magnetosphere. Both compression and expansion events cause order-of-magnitude increases in ion drag force and a factor-of-two increase in the rate of advection of momentum. These result in thermospheric temperature changes >25 K. For auroral emissions, we find that transient compressions double main oval emission and shift the location of the oval ~0.2 ° poleward whilst transient expansions do not significantly change main oval emission but shift its location ~1 ° equatorward.

Keywords:
Jupiter, magnetosphere, thermosphere, angular momentum, transience

---

[*] Corresponding author: Tel.: +44 (0)20 7679 4349; fax: +44 (0)20 7679 2328.
Email address: `japheth.yates.09@ucl.ac.uk` (J. N. Yates)

Preprint submitted to Planetary and Space Science *January 17, 2013*

1. Introduction

The interaction between the Jovian magnetosphere and ionosphere is complex. The current systems which connect the planet's ionosphere and magnetosphere are controlled by a feedback mechanism involving the rotation of magnetospheric plasma, the conductance of the ionosphere and the wind system prevailing in the thermosphere (upper atmosphere). Several studies, however, have made substantial progress in modelling this interaction (Hill, 1979; Pontius, 1997; Cowley and Bunce, 2003a,b; Nichols and Cowley, 2004; Cowley et al., 2005, 2007; Ray et al., 2010, 2012). The models of Cowley and Bunce (2003a,b); Nichols and Cowley (2004) were primarily used to study the interaction of the inner and middle magnetosphere and how these regions couple with the Jovian ionosphere; Cowley et al. (2005) and Cowley et al. (2007) expanded on the former studies by incorporating simplified models for the outer magnetosphere and polar cap region, and thus coupling the 'entire' magnetosphere to the ionosphere.

In addition, Cowley and Bunce (2003a,b) and Cowley et al. (2007) investigated how the coupled magnetosphere-ionosphere (M-I) system interacts with the solar wind - specifically, transient variations in the solar wind dynamic pressure which cause compressions and expansions of the magnetosphere. These models have made realistic predictions regarding the corresponding response of magnetospheric and ionospheric currents, plasma angular velocity profiles and auroral emission (both in terms of the intensity of emission and its location in the ionosphere). Many of these model predictions are supported by observations and complementary theoretical studies such as Nichols et al. (2009); Clarke et al. (2009) and Southwood and Kivelson (2001). None of these aforementioned studies, however, have accounted for the dynamics of the Jovian thermosphere. In these studies the thermosphere is assumed to have an angular velocity Ω_T, independent of altitude, which is derived from a constant 'slippage factor', K, given by

$$K = \frac{(\Omega_J - \Omega_T)}{(\Omega_J - \Omega_M)}. \tag{1}$$

In this expression Ω_J ($1.76\times10^{-4}\,\mathrm{rad\,s^{-1}}$) is the angular velocity of the planet and Ω_M is the angular velocity of the magnetospheric region conjugate to the thermosphere. This ensures the ordering $\Omega_J > \Omega_T > \Omega_M$, for a steady state, where angular momentum is transferred from ionosphere to magnetosphere.

Smith and Aylward (2009) expanded further on the current body of M-I models by coupling a simplified magnetosphere model with an azimuthally symmetric Global Circulation Model (GCM) of Jupiter. Their approach allowed for the self-consistent calculation of the Jovian thermospheric angular velocity, in a coupled M-I system which had reached a steady state.

The study by Smith and Aylward (2009) produced some notable results such as:
i) Angular momentum transfer: meridional advection of momentum, rather than vertical viscous transport, is the main mechanism for transferring angular momentum in the high latitude thermosphere.
ii) Thermospheric super-corotation: the thermosphere super-corotates (Ω_T=1.05 Ω_J) throughout those latitudes (∼65−73 °) where it magnetically maps to the middle magnetosphere (∼6−25 $\mathrm{R_J}$).
iii) Distribution of heat: the simulated thermospheric winds develop two main cells of meridional flow, which cool lower latitudes ($\lesssim$75 °) whilst heating the polar regions ($\gtrsim$80 °).

Yates et al. (2012) used the Smith and Aylward (2009) model to study the influence that solar wind had on the steady-state thermospheric flows of Jupiter. They found that ionospheric and magnetospheric currents, thermospheric powers, temperature and auroral emission (by proxy of field-aligned current (FAC)) all showed an increase with decreasing solar wind dynamic pressure (from 0.213 nPa to 0.021 nPa (Joy et al., 2002)). In particular, ion drag (which changes kinetic energy) and Joule heating were shown to increase by $\lesssim$200 %, which led to a corresponding ∼135 K increase in thermospheric temperature.

Southwood and Kivelson (2001) suggested that, after a magnetospheric compression, there would be an increase in the degree of magnetospheric plasma corotation (i.e. the quantity $(\Omega_J - \Omega_M)$ would decrease), and this would consequently lead to a sizeable decrease in M-I coupling currents and auroral emission. They also argued that the reverse would be true for a magnetospheric expansion. Modelling by Cowley et al. (2007) and Yates et al. (2012) confirmed these predictions, provided the system is given enough time to achieve steady-state. On the other hand, the study of Cowley et al.

(2007) simulated the short-term response of the system to very rapid magnetospheric compressions and expansions. This short-term behaviour was found to exhibit very different properties to that of the steady state. For rapid compressions ($\lesssim$3 hours), the conservation of plasma angular momentum causes the magnetosphere to super-corotate compared to the planet and thermosphere. The flow shear between the thermosphere and magnetosphere, represented by $(\Omega_T - \Omega_M)$, is now negative and leads to current reversals at co-latitudes that are magnetically mapped to the middle and outer magnetospheres ($\sim$10$-$17$\,^\circ$). Negative flow shear also causes energy to be transferred from the magnetosphere to thermosphere; in contrast to the steady-state, where energy is transferred from the thermosphere to the magnetosphere, in order to accelerate magnetospheric plasma towards corotation. For transient expansions, Cowley et al. (2007) showed that Ω_M decreases but the flow shear increases, leading to a $\sim$500 % increase in the intensity of M-I currents (for an expansion from a dayside magnetopause radius of 45 $\mathrm{R_J}$ to 85 $\mathrm{R_J}$, R_J=71492 km).

For transient events, where the magnetopause is displaced by $\sim$40 $\mathrm{R_J}$, Cowley et al. (2007) predict differing auroral responses dependent on the nature of the event, i.e compression or expansion. For compressions, electron energy flux at the open-closed field line boundary (polar emission) increases by two orders of magnitude, whilst the main emission decreases by half. In the expansion case, there is a 30-fold increase in main emission mapping to the middle magnetosphere, whilst polar emission decreases to $\sim$2 % of its steady-state value. Recent observations of auroral emission by Clarke et al. (2009) show a factor of two increase in total ultraviolet (UV) auroral power, near the arrival of a solar wind compression region, typically corresponding to an increase in solar wind dynamic pressure of $\sim$0.01$-$0.3 nPa. Furthermore, Nichols et al. (2009) showed, using the same HST images as in Clarke et al. (2009), that this increase in auroral emission consists of approximately even contributions from the so-called ‘main oval’ and the high-latitude polar emission. Nichols et al. (2009) also showed that the location of the ‘main oval’ shifted polewards by $\sim$1$\,^\circ$ in response to solar wind pressure increase of an order of magnitude. For a rarefaction region in the solar wind, an order of magnitude decrease in solar wind pressure, Clarke et al. (2009) observed little, if any, change in auroral emission.

In this study, we use the Yates et al. (2012) model, ‘JASMIN’, to estimate the response of Jovian thermospheric dynamics to transient changes in the solar wind dynamic pressure and, consequently, magnetospheric size. By transient, we mean changes on time scales $\lesssim$3 hours, where the angular momentum of the magnetospheric plasma is approximately conserved (Cowley et al., 2007). The time scales required for changes in the M-I currents to affect Ω_M are much longer, $\sim$10$-$20 hours. We investigate the response of M-I coupling currents and thermospheric dynamics to our time-dependent profiles of plasma angular velocity in the magnetosphere. We employ different $\Omega_M(\rho_e, t)$ profiles (ρ_e represents equatorial radial distance; t denotes time) to represent compressions and expansions of the middle magnetosphere. A companion paper to this one (Yates et al, 'Effect of transient solar wind pulses on atmospheric heating at Jupiter', in preparation, 2012c. Henceforth Paper 2.) will present results on the effect of these transient events on atmospheric heating and auroral emission of the coupled system. In the present study, we focus on the dynamic response of the thermosphere. These will be the first studies to investigate how transient variations in solar wind pressure influence both magnetospheric and thermospheric properties of the Jovian system, and to use a realistic GCM to represent the thermosphere.

In section 2 we summarise the scientific background needed for this study, as well as model details and the limitations with our current model. In sections 3 and 4 we present our findings for the transient compression and expansion scenarios respectively. We discuss our findings and conclusions in sections 5 and 6.

2. Scientific Background

2.1. Time-dependence of the Jovian system

Variations in magnetic field, plasma angular velocity and thermospheric flow patterns due to solar wind pressure changes present challenges for modelling the Jovian system. Various time-scales, such as those associated with M-I coupling, compression or expansion of the magnetosphere and thermospheric response, need to be considered. The studies by Cowley and Bunce (2003a,b) and Cowley et al. (2007) are among the few to have addressed these issues, using the simplifying approximations discussed hereafter.

i) M-I coupling time scale: The neutral atmosphere transfers angular momentum to the magnetosphere along magnetic field lines, in order to accelerate the radially outflowing magnetospheric plasma towards corotation. The time-scale on which this angular momentum is transferred has been estimated by Cowley and Bunce (2003a) to be $\sim 5-20$ hours.

ii) Compression (and expansion) of the magnetosphere: Large changes in magnetospheric size ($\sim 40\,\mathrm{R_J}$) can occur when the Jovian magnetosphere encounters a sudden change in solar wind dynamic pressure, such as would be caused by a Coronal Mass Ejection (CME) or Corotating Interaction Regions (CIR). Cowley and Bunce (2003a) and Cowley et al. (2007) considered compressions (and expansions) occurring over $\sim 2-3$ hours, and were thus able to assume conservation of plasma angular momentum when calculating the response of the M-I system.

iii) Thermospheric response time: The thermosphere and magnetosphere are coupled together via ion-neutral collisions in the ionosphere; therefore a change in plasma angular velocity would cause a corresponding change in the thermosphere's effective angular velocity. Recent models for the thermospheric response are generally divided in two scenarios: (i) A system where the thermosphere responds promptly, on the order of a few tens of minutes (Millward et al., 2005), and (ii) a system where the thermosphere responds on the order of two days and, as such, is essentially unresponsive to transient events (Gong, 2005). However, in this study, we do not make a distinction between thermospheric response models. We simply allow the GCM to react to the imposed changes in plasma angular velocity assumed for the transient compressions and expansions, thus allowing a realistic, thermospheric response to these changes.

2.2. Magnetosphere model

The quiescent magnetosphere model used herein is axisymmetric and consists of two parts:

i) An equatorial magnetic field profile, taken from Nichols and Cowley (2004), who employed the following function, which is a fit to field profiles derived from spacecraft magnetic data from the Pioneer and Voyager missions (presented by Connerney et al. (1981) and Khurana and Kivelson (1993))

$$B_{ze}(\rho_e) = -B_o \left(\frac{R_J}{\rho_e}\right)^3 \exp\left[-\left(\frac{\rho_e}{\rho_{eo}}\right)^{5/2}\right] - A\left(\frac{R_J}{\rho_e}\right)^m , \qquad (2)$$

where B_o=3.335 $\times 10^5$ nT, ρ_{eo}=14.501 $\mathrm{R_J}$, A=5.4 $\times 10^4$ nT, m=2.71 . Eq. (2) represents a southward pointing field, with negative z (vertical) component. Associated with this field profile is a flux function, which represents the magnetic flux integrated between a given equatorial radial distance ρ_e and infinity

$$F_e(\rho_e) = F_\infty + \frac{B_o R_J^3}{2.5\rho_{eo}} \Gamma\left[-\frac{2}{5}, \left(\frac{\rho_e}{\rho_{eo}}\right)^{5/2}\right] + \frac{A R_J^2}{m-2}\left(\frac{R_J}{\rho_e}\right)^{m-2} , \qquad (3)$$

where $F_\infty \approx 2.841 \times 10^4$ nT $\mathrm{R_J^2}$, and $\Gamma(a,z) = \int_z^\infty t^{a-1} e^{-t} dt$ is the incomplete gamma function.

Surfaces of constant flux function define shells of magnetic field lines with common equatorial radii and ionospheric co-latitude. These surfaces also allow for the magnetic mapping from the equatorial plane of the magnetodisc (middle magnetosphere) to the ionosphere. This mapping requires an ionospheric flux function equation $F_i(\theta_i)$ and the equality $F_i(\theta_i) = F_e(\rho_e)$, which represents the mapping between the ionospheric co-latitude θ_i and the equatorial radial distance ρ_e to which the corresponding magnetic field line extends (Nichols and Cowley, 2004).

$$F_i = B_J \rho_i^2 = B_J R_i^2 \sin^2\theta_i . \qquad (4)$$

where B_J is the equatorial magnetic field strength at the planet's surface and ρ_i is the perpendicular distance to the planet's magnetic/rotation axis ($\rho_i = R_i \sin\theta_i$, where R_i is the ionospheric radius. We adopt B_J=426400 nT (Connerney et al., 1998), and R_i=67350 km (Cowley et al., 2007). Note $R_i < R_J$ due to polar flattening at Jupiter.

ii) A profile for the angular velocity of the magnetospheric plasma. Here, we follow Cowley et al. (2007) who commence with a 'quiescent' solution for Ω_M, given by the steady-state solution of the Hill-Pontius equation (Hill, 1979; Pontius, 1997):

$$\frac{1}{\rho_e}\frac{d}{d\rho_e}\left(\rho_e^2\Omega_M\right) = \frac{8\pi\Sigma_P F_e|B_{ze}|}{\dot{M}}\left(\Omega_T - \Omega_M\right), \tag{5}$$

where $\dot{M}$=1000 kg s^{-1} is the assumed mass outflow rate from the Io torus. The Hill-Pontius equation balances torques caused by the outward diffusion of the disc plasma and the $\boldsymbol{J}\times\boldsymbol{B}$ force associated with the magnetosphere-ionosphere coupling currents. As in Cowley et al. (2007), we assume for the purposes of solving Eq. (5) a uniform height integrated Pedersen conductance Σ_P=0.5 mho.

We now discuss the required changes to our 'quiescent' magnetosphere model, in order to predict the behaviour of the magnetic field due to transient magnetospheric compressions and expansions. We use the principle of magnetic flux conservation as described by Cowley et al. (2007). A uniform southward (resp. northward) perturbation field ΔB_z, is added to the initial, quiescent field (obtained using Eq. (2)), at every time step during the transient compression (resp. expansion) from an initial magnetodisc radius R_{MMO}. ΔB_z can be calculated, as a function of magnetodisc radius $R_{MM}(t)$ (at each time step t) using the flux conservation condition employed by Cowley et al. (2007)

$$-\pi R_{MM}(t)^2\Delta B_z = 2\pi\left(F_e\left(R_{MM}(t)\right) - F_e\left(R_{MMO}\right)\right). \tag{6}$$

Solving for ΔB_z gives

$$\Delta B_z = \frac{-2\Delta F}{R_{MM}(t)^2}, \tag{7}$$

where $\Delta F = F_e\left(R_{MM}(t)\right) - F_e\left(R_{MMO}\right)$ and ΔB_z<0 for compressions and ΔB_z>0 for expansions.

Plasma angular momentum conservation is used to obtain transient plasma angular velocity profiles $\Omega_M(\rho_e, R_{MM}(t))$ during the simulated compressions and expansions of the system. This is discussed in section 2.5.

2.3. Magnetosphere-ionosphere coupling

In this section we discuss the effect of coupling the magnetosphere and ionosphere together. The meridional electric field in the rest frame of the thermosphere may be written as:

$$E_\theta = B_i \rho_i \left(\Omega_T - \Omega_M\right), \tag{8}$$

where B_i is the magnitude of the (assumed) radial ionospheric magnetic field (B_i=$2B_J$).

The combination of electric field, magnetic field and ion-neutral collisions causes Pedersen currents to flow in the ionosphere, mainly perpendicular to the direction of the planetary magnetic field. These ionospheric currents form part of a larger current circuit which includes the radial current flowing in the magnetodisc and the FAC flowing along the magnetic field lines. The height integrated Pedersen current density i_P and its azimuthally integrated form $I_P(\theta_i)$ are (Cowley et al., 2007; Smith and Aylward, 2009)

$$i_P = \rho_i \Sigma_P \left(\Omega_T - \Omega_M\right) B_i, \tag{9}$$

and

$$I_P(\theta_i) = 2\pi \rho_i^2 \Sigma_P \left(\Omega_T - \Omega_M\right) B_i, \tag{10}$$

where Ω_T is a weighted average, computed over altitude, of the angular velocity of the thermosphere. For a more detailed description of this the reader is referred to Yates et al. (2012) and Smith and Aylward (2009).

The height-integrated radial current density in the magnetodisc is denoted by i_ρ and can be obtained using Eq. (9) under the assumption of current continuity (zero divergence of current density). We have (Nichols and Cowley, 2004; Smith and Aylward, 2009):

$$\rho_e i_\rho = 2\rho_i i_P, \tag{11}$$

$$I_\rho = 8\pi \Sigma_P F_e \left(\Omega_T - \Omega_M\right), \tag{12}$$

where I_ρ is the azimuthally integrated disc current.

The third and final component of our M-I current circuit is the FAC density. $j_{||i}(\theta_i)$ represents the FAC density at the ionospheric footpoint (at co-latitude θ_i) of the respective field lines. This current density is obtained from the horizontal divergence of the Pedersen current:

$$j_{||i}(\theta_i) = -\frac{1}{2\pi R_i^2 \sin\theta_i}\frac{dI_P}{d\theta_i}, \tag{13}$$

where the sign of $j_{||i}(\theta_i)$ indicates FAC direction (positive upward from planet). Eq. (13) corresponds to the northern hemisphere, where the magnetic field points radially outward (approximately, in auroral region) (Cowley et al., 2007).

The M-I coupling also produces a drag on the thermosphere, due to the ion-neutral collisions. Huang and Hill (1989) showed that this drag results in the thermosphere lagging behind planetary corotation and that this lag can be quantified with a 'slippage parameter' K, given in Eq. (1). K thus represents the 'slippage' of the neutrals from rigid corotation. The use of GCMs in Yates et al. (2012) and Smith and Aylward (2009) showed that K varies considerably with ionospheric location - an effect that is often neglected in magnetospheric studies.

2.4. Thermospheric dynamics

The thermosphere model used in this study is a GCM which solves the non-linear Navier-Stokes equations of energy, momentum and continuity, using explicit time integration (Müller-Wodarg et al., 2006). The Müller-Wodarg et al. (2006) GCM was created for Saturn's thermosphere, and later modified for Saturn and Jupiter in Smith and Aylward (2008) and Smith and Aylward (2009) respectively. It is this modified GCM that we use in this study. The model assumes azimuthal symmetry, and is thus two-dimensional (pressure/altitude and latitude).

The axisymmetric Navier-Stokes equations are solved in the pressure coordinate system, providing time-dependent distributions of thermospheric wind and temperature. The zonal and meridional momentum equations, forming the basis of this particular study are (see also Achilleos et al. (1998); Tao et al. (2009)):

$$\frac{\partial u_\phi}{\partial t} = -\frac{u_\theta}{R_J}\frac{\partial u_\phi}{\partial \theta}\bigg|_p - w\frac{\partial u_\phi}{\partial p} + F_{vis_\phi} + F_{cor_\phi} + F_{ion_\phi}, \tag{14}$$

$$\frac{\partial u_\theta}{\partial t} = -\frac{u_\theta}{R_J}\frac{\partial u_\theta}{\partial \theta}\bigg|_p - w\frac{\partial u_\theta}{\partial p} - \frac{g}{R_J}\frac{\partial z}{\partial \theta}\bigg|_p + F_{vis_\theta} + F_{cor_\theta} + F_{ion_\theta}, \tag{15}$$

where u_ϕ and u_θ are the respective zonal (positive eastwards) and meridional (positive southwards) components of neutral wind velocity, ϕ represents azimuthal direction, w ($w = dp/dt$) is the convective time derivative of the atmospheric pressure p, z is the altitude above the 1 bar level and g (g=22.88 m s^{-2}) is the acceleration due to gravity (assumed uniform). The remaining acceleration terms are due to the viscosity (F_{vis}), fictitious forces (sum of Coriolis and curvature terms in the model's corotating reference frame, F_{cor}) and ion drag (F_{ion}), and are evaluated as follows:

$$\mathbf{F_{vis}} = \frac{\eta}{\rho_m}\nabla_p^2\mathbf{u} + g^2\frac{\partial}{\partial p}\left(\eta\rho_m\frac{\partial \mathbf{u}}{\partial p}\right), \tag{16}$$

$$\mathbf{F_{ion}} = \frac{1}{\rho_m}\mathbf{j}\times\mathbf{B}, \tag{17}$$

$$\mathbf{F_{cor\theta}} = \frac{u_\phi^2\cot\theta}{r} - \frac{u_r u_\theta}{r} - 2\Omega_J u_\phi\cos\theta, \tag{18}$$

$$\mathbf{F_{cor\phi}} = -\frac{u_\phi u_\theta\cot\theta}{r} - \frac{u_\phi u_r}{r} + 2\Omega_J u_\theta\cos\theta, \tag{19}$$

where $\mathbf{u}$ is the neutral velocity vector, η is the coefficient of viscosity, ρ_m is the mass density, r is the radial distance to the centre of Jupiter, $\mathbf{j}$ is the ionospheric horizontal current, $\mathbf{B}$ is the local magnetic field at the thermosphere/ionosphere and u_r is the vertical neutral wind velocity. Eqs. (14 - 19) are used by our model to calculate horizontal momentum terms for Jupiter's thermosphere.

2.5. Obtaining the transient plasma angular velocity

We now discuss the calculation of plasma angular velocity once the model has entered the transient regime i.e. once our initial, steady-state system begins to undergo a transient compression/expansion of the magnetosphere.

Our method of calculating transient plasma angular velocities follows that of Cowley et al. (2007). Prior to the rapid compression or expansion, the system exists in a steady state, with plasma angular velocity $\Omega_M(\theta_i, t{=}0)$ as a function of co-latitude θ_i and time t. Using the magnetic mapping method discussed in section 2.2, the equatorial radial distance $\rho_e(\theta_i, t{=}0)$ of the local field line can be found. The arrival of the solar wind pulse or rarefaction causes the magnetosphere to compress or expand by several tens of R_J (typical choice for the simulations) and the model enters the transient (time-dependent) regime. Thus, a given co-latitude θ_i now maps to a new radial distance $\rho_e(\theta_i, t)$. If, as discussed in section 2.1, the solar wind pulse causes perturbations that occur on sufficiently small time scales ($\sim$2$-$3 hours), we can assume that plasma angular momentum is approximately conserved. The plasma angular velocity profile throughout the 'pulse' in solar wind pressure is then given by:

$$\Omega_M(\theta_i, t) = \Omega_M(\theta_i, t{=}0) \left(\frac{\rho_e(\theta_i, t{=}0)}{\rho_e(\theta_i, t)} \right)^2, \tag{20}$$

where the notation $t{=}0$ and t denote the initial (steady-state) and transient state (at each time-step throughout the event) respectively.

For this study, the time evolution of solar wind dynamic pressure, and thus magnetodisc size, is represented by a Gaussian function. $R_{MM}(t)$ represents the magnetodisc radius as a function of time and is given by

$$R_{MM}(t) = Ae^{-\frac{(t-t_o)^2}{2\Delta t^2}} + R_{MMO}, \tag{21}$$

where $A{=}R_{MM}(t_o) - R_{MMO}$ and is the amplitude of the corresponding curve, $R_{MM}(t_o)$ is the maximum or minimum radius, t_o is the time at which $R_{MM}(t){=}R_{MM}(t_o)$ (90 minutes after pulse start time t_s), and Δt controls the width of the 'bell' (obtained using $(2/3)(t_o - t_s) = 2\sqrt{2\ln 2}\ \Delta t$). After achieving steady-state, we run the model for a single Jovian day, transient mode is then initialised 3 hours prior to the end of the Jovian day (and model runtime). Profiles of $R_{MM}(t)$ for compressions and expansions are shown in Fig. 1.

As indicated in Fig. 1, the simulated pulse lasts for a total of three hours, after which the magnetodisc returns to its initial size. This is represented by the black solid (compression) and dot-dashed (expansion) lines. The grey dashed line indicates the point of maximum compression/expansion (at t=t_o) where we take a 'snapshot' of model outputs in order to investigate the thermospheric response midway through the transient pulse (henceforth, this phase of the event is referred to as 'half-pulse').

As in Yates et al. (2012), we divided the magnetosphere into four regions: region I, representing open field lines of the polar cap; region II containing the closed field lines of the outer magnetosphere; region III (shaded in figures) is the middle magnetosphere (magnetodisc) where we assume the Hill-Pontius equation is valid for steady-state conditions. Region IV is the inner magnetosphere (which is assumed to be fully corotating in steady state). Region III is our main region of interest throughout this study since it plays a central role in determining the morphology of auroral currents.

Plasma velocities are shown in Fig. 2 (thin lines) along with their corresponding thermospheric angular velocities (thick lines). Fig. 2a shows angular velocity profiles pertaining to the transient compression scenario. The starting configuration (steady-state) is indicated by solid lines and is henceforth, referred to as 'case CS' (pre-Compression Steady-state). Halfway through the pulse, when the magnetodisc radius is a minimum, angular velocity profiles are represented by dashed lines and will be referred to as case CH (Compression Half-pulse). Case CF (Compression Full-pulse) profiles are indicated by dot-dashed lines and represent the state of the system after the pulse subsides. In Fig. 2a, we see an average of $\sim$3 % increase in peak Ω_T in response to the transient compression event. This is small compared to the factor of two increase in peak Ω_M (for case CH). The significant difference in response between the thermosphere and magnetosphere is due to the larger mass of the neutral thermosphere and thus, its greater resistance to change (inertia). There is significant super-corotation of the magnetodisc plasma throughout most of regions IV and III, midway through the compression. Plasma rotating faster than both the thermosphere and deep planet creates a reversal of currents and angular momentum transfer between the ionosphere and magnetosphere (Cowley et al., 2007). Thus angular momentum is transported from the magnetosphere to the thermosphere, where rotation rate increases from its initial state. After the subsidence of the pulse, the magnetosphere returns to its initial size and thus, the Ω_M profile for case CF is equal to that of CS at all latitudes. The same cannot be said for the thermospheric angular velocities; the CF thermosphere rotates slightly faster ($\sim$2 % at maximum Ω_T) for parts of regions III and I and all of region II. This comparison highlights the difference in response between the thermosphere and magnetosphere to the prescribed changes in solar wind pressure.

Fig. 2b shows angular velocity profiles corresponding to the transient expansion scenario. Like the compression scenario, we have cases ES (pre-Expansion Steady-state (initial value of R_{MM}=45 R_J)), EH (Expansion Half-pulse) and EF (Expansion Full-pulse) indicated by solid, dashed and dot-dashed lines respectively. The behaviour is very different from the compression: midway through the event (case EH), the magnetodisc plasma sub-corotates to an even greater degree in regions IV and III compared to the initial steady-state case, ES. The thermosphere also sub-corotates to a greater degree, but remains at higher angular velocity than the disc plasma, meaning that current reversal does not occur. Thermospheric angular velocities for cases ES and EF differ slightly, as in the compression scenario i.e due to the greater lag in the thermospheric response time.

Fig. 2 theoretically demonstrates the effect that transient increases and rarefactions in the solar wind dynamic pressure have on both plasma and thermospheric angular velocities. Sections 3 and 4 will discuss the effects on the M-I coupling currents and the global thermospheric dynamics.

2.6. Limitations of our approach

Our approach for obtaining transient solutions for plasma angular velocity is only valid within the middle magnetosphere region, which we take to lie between 4 $\mathrm{R_J}$ and R_{MM}. The 'outer magnetosphere' in our model is a layer between the outer edge of the plasmadisc and the magnetopause. We assume that the angular velocity in this layer is uniform with distance, but dependent on magnetospheric size, as in Yates et al. (2012) for the steady-state, and as in this paper for transient changes. The velocity in the polar cap region is fixed at a constant value of $\sim 0.1\,\Omega_\mathrm{J}$, in accordance with the formula of Isbell et al. (1984). Transient effects on thermospheric velocities, however, are transmitted throughout the higher/polar latitudes (>74 °) of the model Jovian thermosphere. We note that, for the magnetosphere, we do not solve time-dependent equations of motion, we simply use those discussed in section 2.4 and see how they drive transient changes in the thermosphere.

Another limitation to our transient mode is the use of a constant value for the true height-integrated Pedersen conductivity of Σ_P=0.5 mho. At present, enhancements in Σ_P due to auroral precipitation of electrons is only accounted for within our steady-state model (Yates et al., 2012). We do, however, note that this auroral enhancement of the conductivity during a transient event is interesting, likely to be significant and will be incorporated into the model in a future study.

3. Magnetospheric Compressions

In this section we present findings for our transient magnetospheric compression scenario. We show initial, steady state profiles (case CS with R_{MM}=85 $\mathrm{R_J}$), 'half-pulse' profiles (case CH with R_{MM}=45 $\mathrm{R_J}$) and 'full-pulse' profiles (case CF with R_{MM}=85 $\mathrm{R_J}$). The transient event lasts for a total of three hours.

3.1. M-I coupling currents

Here we discuss how a transient compression event affects the M-I coupling currents. We compare initial steady-state currents with those calculated at 'half-' and 'full-' pulse intervals; indicated by cases CS, CH and CF respectively.

In the model of Cowley et al. (2007) a transient compression of the magnetosphere causes significant super-corotation of the magnetodisc plasma, compared to both the thermospheric and planetary angular velocities. This leads to a current reversal throughout the middle magnetosphere (region III). Fig. 3a shows the variation of azimuthally integrated radial current with equatorial radial distance for cases CS, CH and CF. The solid line shows case CS, whilst the dashed and dot-dashed lines show the respective half- and full-pulse cases (CH and CF). Comparing cases CS and CH we see very different profiles. The expected current reversal (negative I_ρ), for the compressed system, is caused by the super-corotation of the magnetosphere compared to the thermosphere (see section 2.5); thus, the shear $(\Omega_T - \Omega_M)$ is negative and creates disc currents which flow radially planetward (reversed), instead of outward (as in steady-state). The profile for case CF resembles that of CS but with larger radial current ($\sim$20 % on average) at all equatorial radii. The differences between these two cases are attributed to the response of the thermosphere to the transient pulse. At full-pulse, $\Omega_M(CF)$=$\Omega_M(CS)$ but $\Omega_T(CF)\neq\Omega_T(CS)$ as the thermosphere has not had sufficient time to settle back to a steady-state (due to its large inertia, as discussed in section 2.5). Although this is a subtle example of the atmospheric modulation of auroral currents, future simulations will aim at further exploring how this effect changes within the parameter space of the pulse duration and its change in solar wind pressure.

Fig. 3b shows the azimuthally integrated Pedersen current I_P in the high latitude ionosphere for cases CS, CH and CF. Conjugate magnetospheric regions are labelled and separated with dotted black lines. The line style code is the same as Fig. 3a. I_P is half of the radial current I_ρ flowing through the magnetically conjugate location in the plasmadisc (continuity of current between disc and two planetary hemispheres). Thus, in region III, the trends in Fig. 3b reflect those in Fig. 3a. For example, in case CH, where I_P is negative (region III), the Pedersen current flows polewards instead of equatorwards, as in steady-state. In region II, we have fixed Ω_M at a value depending on magnetodisc size (Cowley et al., 2005). This causes the difference in I_P between case CS and CH in region II. The analogous difference between cases CS and CF is, once again, due to the lag in thermospheric response as discussed above. In region I, we select a fixed value of $0.10\,\Omega_\mathrm{J}$, over all cases, for Ω_M in concordance with Isbell et al. (1984), resulting in minimal differences between the current profiles in this region.

Fig. 4 shows FAC density as a function of latitude (computed from the horizontal divergence of I_P) for cases CS, CH and CF. The line style code is the same as for Fig. 3, and, for comparison, the latitudinal size of a Hubble Space Telescope (HST) ACS-SBC pixel (0.03x0.03 arc sec) is indicated by the dark gray rectangle. Comparing cases CS and CF in region III, with increasing latitude (moving polewards), there is one FAC density peak and one trough for each case. The peaks are located at $\sim$74 °, corresponding to the 'main auroral oval'. The trough, in both cases is located at the region III/II boundary. In regions II and I, FAC density profiles remain slightly negative. Peaks in FAC arise from strong spatial gradients in Ω_M (Ω_M decreases by $\sim$78 % across $\sim$2 °), and consequently, flow shears located at or near magnetospheric region boundaries. The troughs at the region III boundary are due to large spatial gradients in Ω_M and Σ_P encountered as we traverse this boundary (Yates et al., 2012). Given the FAC profiles for cases CS and CF, we would expect to see aurorae of similar intensity (CF being $\sim$16 % more intense than CS), corresponding to the main oval only, at $\sim$74 ° latitude.

Case CH, on the other hand, is more interesting, as it shows the largest deviation from steady state. The CH FAC density profile is initially directed downwards at latitudes up to ∼73 °. At this location, the FAC becomes positive and peaks at ∼74 °. FAC then decreases to roughly constant negative values throughout regions II and I, but with a large, $\sim 0.2\,\mu\,\mathrm{A\,m^{-2}}$ peak at the region II/I boundary due to a corresponding change in Ω_M. In terms of auroral emissions, we would expect relatively dark regions where the FAC is negative. The factor of two increase in peak FAC (at ∼74 °) compared to cases CS and CF suggests a much brighter and somewhat narrower 'main auroral oval' for the most compressed configuration of the magnetosphere. Observations reported by Clarke et al. (2009) and Nichols et al. (2009) indicate that the UV auroral emission increases in brightness by factors of two, in response to rapid increases in solar wind dynamic pressure of the order of ∼0.01−0.3 nPa. Our results also suggest the possibility of observable polar emission located at the open-closed field line boundary (region II/I). However, this conclusion is strongly dependent on the assumptions made for the outer magnetospheric plasma flow. The latitudinal location of the main peak has also shifted polewards by ∼0.2 ° in the CH profile, which has been seen in modelling by Yates et al. (2012). Observations by Nichols et al. (2009) have seen poleward shifts in main oval emission by up to ∼1 ° corresponding to the arrival of solar wind shocks.

We briefly compare FAC densities from case CH with transient results from Cowley et al. (2007) (compression from $85-45\,\mathrm{R_J}$). Despite a resemblance in FAC profiles, peak FACs in the magnetodisc (region III) are ∼2.5 times larger in case CH than the equivalent case (with a responsive thermosphere) in Cowley et al. (2007). The peak FACs in case CH, are actually closer to those in Cowley et al. (2007)'s non-responsive thermosphere compression case. This suggests that, the thermosphere (represented by a GCM) in our study lies somewhere in between a responsive and non-responsive thermosphere (although closer to the latter, for the pulse parameters assumed).

For completeness, we also calculated M-I coupling currents for the case of a non-responsive thermosphere (Gong, 2005). To do this, we assume that $\Omega_T{=}\Omega_T(CS)$ throughout the entire transient event. In this non-responsive thermosphere scenario, there is an average increase in M-I currents of ∼20 % midway through the pulse compared to case CH (obtained using GCM). At full-pulse, however, the non-responsive case has M-I currents that are on average ∼12 % smaller than currents in case CF. These differences between a non-responsive thermosphere and a responsive one (GCM), are related to the flow shear between thermosphere and magnetosphere; which, is maximal (resp. minimal) at half-pulse (resp. full-pulse) when using a non-responsive thermosphere.

In summary, the FAC densities in Fig. 4 suggest that a transient compression will cause a narrowing and poleward shift in the location of the main auroral oval (∼0.2 °), as well as an increase by a factor of ∼2 in peak brightness. These predictions are of similar order to HST observations carried out by Nichols et al. (2009) and Clarke et al. (2009).

3.2. Thermospheric dynamics

In this section, we discuss the thermospheric response to the simulated transient magnetospheric compressions. We present the variation of azimuthal and meridional thermospheric flows and temperature distribution. We then proceed to interpret the model outputs, in the context of the dominant acceleration terms contributing to the evolution of momentum.

Smith et al. (2007), Smith and Aylward (2009) and Yates et al. (2012) showed that in the Jovian auroral thermosphere, there are two main steady-state flow patterns:

i) Low-altitude (<600 km*)*: Here, ion drag acceleration becomes strong due to the Pedersen conductivity layer (maximum value of $0.1163\,\mathrm{mho\,m^{-1}}$ at ∼370 km). An imbalance is created between ion drag, Coriolis and pressure gradient terms; thus, giving rise to advection of momentum which, restores equilibrium in this low altitude region. This results in mostly sub-corotational, poleward flow as shown in Fig. 5a.

ii) High-altitude (>600 km*)*: Conditions are quite different at high-altitudes, meridional Coriolis and pressure gradient accelerations are essentially balanced, whilst terms such as ion drag, advection and zonal Coriolis are small and insignificant. This creates a 'jovistrophic' condition, whereby flow is directed very slightly equatorwards and is sub-corotational, as shown in Fig. 5b.

Fig. 6 shows the altitude and latitude variation of azimuthal and meridional thermospheric velocities and thermospheric temperature for the transient compression cases. Figs. A.1 - A.3 (Appendix A) show the corresponding zonal and meridional acceleration terms associated with each case. From left to right, the columns in Fig. 6 and Figs. A.1 - A.3, represent cases CS, CH and CF respectively.

Figs. 6a-c shows the variation of thermospheric azimuthal velocity, in the corotating reference frame, in the high latitude thermosphere for cases CS-CF. Positive (resp. negative) values of azimuthal velocity indicate super (resp. sub)-corotating regions. The direction of meridional flow is indicated by the black arrows, the locus of rigid corotation is indicated by the white line, strong super-corotation is indicated by the black contour, strong sub-corotation is indicated by the dashed white contour, and the magnetospheric regions are labelled and separated by black dotted lines. Zonally, there are two prominent features in our transient compression cases: i) a low altitude small super-corotating jet, centred at ∼72 °, and ii) a large sub-corotating jet, from region III - I (blue region in Figs. 6a-c). Figs. 6d-f shows the variation of meridional flows in the high latitude thermosphere for our transient compression cases. Magnetospheric labels, locus of corotation and arrows are the same as in Figs. 6a-c. These figures, show the meridional flow pattern in the thermosphere, as well as, localised accelerated regions (red/brown hues).

As discussed in Smith and Aylward (2009) and Yates et al. (2012), the super-corotational jet in case CS (Fig. 6a) is created by a small excess in the zonal Coriolis and advection momentum terms compared to the ion drag term (see leftmost column in Fig. A.1). At low altitude, Coriolis force is primarily directed eastwards and unopposed can promote super-corotation in the neutrals. The large sub-corotational jet is caused by the drag of the sub-corotating magnetosphere on the thermosphere. Zonal flows are, for the most part, sub-corotational and momentum terms are balanced in case CS as it is in steady-state. Meridionally, momentum is balanced mainly between Coriolis and pressure gradient terms (see first column of Figs. A.2), except at low altitudes where ion drag is present (due to conductivity layer) which leads to the advection of momentum and accelerated poleward flows as seen in Fig. 6d. These steady-state flow patterns are as shown in Fig. 5.

Zonal flows for case CH (see Fig. 6b), at first glance seem similar to those of case CS, but there is a factor of two increase in the zonal velocity within the region of super-corotation, as well as an increase in latitudinal size of the super-corotating jet. The large, sub-corotational jet remains roughly unchanged but the overall degree of sub-corotation has decreased i.e. the magnitude of azimuthal velocity has decreased by ~4 %. Meridional flows in Fig. 6e, show two additional local acceleration regions either side of ~73 ° latitude and from altitudes >500 km. In the second column of Figs. A.1 - A.3, the thermosphere has undergone significant changes in both zonal and meridional momentum terms. The most pronounced of these are in the ion drag subplots (Figs. A.1b and A.2b), where these terms have changed sign. Therefore, ion drag now acts in the opposite direction compared to steady-state. This results from the current reversal discussed in section 3.1. The increase in super-corotation is mainly caused by eastwards ion drag, which is now larger than both Coriolis and advection terms in region III. Fig. A.2k shows that the local acceleration regions (in Fig. 6e) primarily result from meridional advection of momentum created to balance the non-equilibrium state of the thermosphere (at the half-pulse phase). The direction of flow (arrows) has also reversed in the lower altitude section of region III. This change is attributed to the reversal of meridional ion drag in this region, which now promotes equatorward flow. These changes in dynamics lead to temperature deviations from case CS of ~ ± 25 K (Fig. 6h).

The thermospheric flows of case CF are in the third column of Fig. 6, and the corresponding zonal and meridional momentum terms are shown in the third column of Figs. A.1 - A.3. The first thing we notice is that the thermosphere's altitudinal profile is highly unusual compared to cases CS and CH; there are peaks and troughs poleward of ~65 ° latitude along the upper boundary of our thermosphere. These result from the large temperature deviations (−40 to +175 K) evident at high altitudes in Fig. 6i. The zonal flows in Fig. 6c, continue to exhibit the general features present in cases CS and CH: i) a large sub-corotational jet in regions II and I and, ii) a small super jet at low altitudes in region III. The zonal momentum terms (third column of Fig. A.1), exhibit a somewhat complex nature - particularly in Coriolis and advection terms (Figs. A.1f and i). These show latitudinal and altitudinal fluctuations between positive and negative momentum terms. The ion drag momentum distribution (Fig. A.1c) is, however, returning to its initial state (case CS, Fig. A.1a). This is not surprising as ion drag is directly linked to the magnetosphere (see Eq. (17)) and as such would respond more quickly to changes in magnetospheric conditions when compared to Coriolis, advection or viscous terms. Meridionally, in Fig. 6f, the number of local accelerated regions poleward of 65 ° latitude, have increased significantly. The direction of meridional flow (black arrows) is similar to that of case CH except for high altitudes in regions III and II, where flow directions change on relatively small spatial scales. This complex flow pattern is directly influenced by meridional ion drag and Coriolis terms (Figs. A.2c and f), where (for example) negative ion drag contours map to equatorward flow whilst positive contours map to poleward flow (schematically shown in Fig. 5). On the other hand, the localised accelerations result from advective terms, which respond to the disequilibrium created by the transient event, and also attempt to re-establish hydrostatic equilibrium (see almost one-to-one mapping of advection contours in Figs. A.2l and 6f).

Fig. 6 and Figs. A.1 - A.3 represent the changes that occur in the thermosphere throughout a transient, magnetospheric compression event. We see that the zonal flow structure of the thermosphere does not change significantly with a transient compression event i.e a large sub-corotational jet and a small super-corotational jet. We note, however, that the degree of corotation is strongest when the magnetodisc radius is minimum. In the meridional direction, numerous local accelerated regions develop as the event progresses, as well as significant deviations from steady-state flow patterns. From Fig. 6 and Figs. A.1 - A.3, we see that thermospheric flows are mostly influenced by changes in ion drag and momentum advection terms.

4. Magnetospheric Expansions

This section presents our findings for a transient magnetospheric expansion event. The initial steady-state (magnetodisc radius of $45\,\mathrm{R_J}$), is expanded to a maximum radius of $85\,\mathrm{R_J}$, before subsequently returning to its initial size. The duration of this expansion event is the same as the compression event i.e. three hours.

4.1. M-I coupling currents

We investigate how a transient expansion (a rarefaction region in the solar wind) affects the M-I coupling currents. We compare initial compressed steady-state currents with those calculated at half- and full-pulse intervals; indicated by cases ES, EH and EF respectively.

Fig. 7a shows azimuthally integrated radial current as a function of equatorial radial distance from Jupiter. Case ES is represented by the solid line, whilst cases EH and EF are represented by dashed and dot-dashed solid lines respectively. The dotted grey line merely emphasises zero radial current. Firstly, we compare case ES with EH. There is a factor of three increase in peak radial current from case ES to EH at the outward edge of the magnetodisc. This increase in I_ρ is caused by the large increase in flow shear between the thermosphere and magnetosphere as shown in Fig. 2b. The I_ρ profile for case EF decreased throughout the magnetodisc region to a peak value $\sim$75 % that of case ES. At radii $\lesssim$20 $\mathrm{R_J}$ there is a small amount of current reversal due to the lag of the thermosphere (see Fig. 2b). If allowed to progress, this reversal would lead to an increase in thermospheric angular velocity towards corotation.

The variation of azimuthally integrated Pedersen current with latitude is shown in Fig. 7b. In region III, the current profiles reflect those seen in Fig. 7a as I_P=0.5 I_ρ. The variation between ES and EH in region II is caused by the different values of Ω_M that we prescribe for this region. Differences between ES and EF are, as stated in section 3.1, due to the lag in the response time of the thermosphere to the transient changes in Ω_M.

FAC densities in the high latitude region are plotted for cases ES, EH and EF in Fig. 8. The line style code is the same in Fig. 7b and the size of an HST ACS-SBC pixel is indicated. Comparing cases ES with EH we see three main differences: i) EH has two peaks in region III (of similar magnitude to the peak in case ES) creating a large area of upward-directed FAC, ii) the magnitude of downward FAC near the region III boundary has increased by a factor of four (from ES to EH) and iii) FAC densities at the region II/I boundary are entirely downward-directed unlike case ES. As the magnetosphere expands, its magnetic field strength and plasma angular velocity decrease. This change in Ω_M (see Fig. 2b) increased the flow shear between the magnetosphere and thermosphere and thus increased the FAC in region III by $\sim$15 %. The strong downward FAC results from the large gradients in Ω_M and Σ_P through the poleward boundary of region III. The lack of a peak at the region II/I boundary is due to the small change in Ω_M as the model traverses these two regions. Case EF shows only small differences with case ES due to the lag in response time of the thermosphere to transient magnetospheric changes.

Comparing case EH FAC densities with the corresponding result from

Cowley et al. (2007) (expansion from $45-85\,\mathrm{R_J}$), we notice a few differences: i) the magnitude of peak FAC in case EH is ∼25 % larger than that in Cowley et al. (2007) and, ii) case EF has no upward FAC at the region II/I boundary, contrary to results in Cowley et al. (2007). These differences emphasise the effect of using a time-dependent GCM for the thermospheric response. For example, the 'double peak' structure in the Region III FACs is due to modulation of current by thermospheric flow.

As in section 3.1, we summarise the differences between the M-I coupling currents discussed above and those which arise if we assume a non-responsive thermosphere; such that $\Omega_T = \Omega_T(ES)$ for the duration of the transient event (Gong, 2005). We find that, for both half- and full-pulse datasets, there is, on average, a ∼20 % increase in the maximum magnitude of M-I currents in the non-responsive thermosphere scenario compared to cases EH and EF (using our GCM). These changes are, once again, linked to the flow shear between the magnetosphere and thermosphere. $\Omega_T(ES)$ is uniformly larger than Ω_T for cases EH and EF (see Fig. 2). As such, the flow shear in the non-responsive scenario will always be greater than the flow shear obtained in the GCM thermosphere.

FAC densities in Fig. 8 suggest that transient expansions will cause a broadening of the main auroral oval, a ∼1 ° equatorward shift in peak emission along with a ∼15 % increase in peak FAC density. These results also suggest a possible darkening in the polar cap regions during the expansion. Observations by Clarke et al. (2009) have seen little, if any change in the brightness of auroral emission close to the arrival of solar wind rarefaction regions whilst changes in main oval location (∼1 °) have been observed by Nichols et al. (2009).

4.2. Thermospheric dynamics

We present thermospheric model outputs associated with transient magnetospheric expansions. We firstly present the variation of azimuthal and meridional thermospheric flows and temperature with altitude and latitude. Their associated momentum terms are then used to assist in the interpretation.

The altitude-latitude variation of azimuthal and meridional thermospheric velocities and temperature are shown in Fig. 9. Figs. B.1 - B.3 show the corresponding zonal and meridional momentum terms. The first column in Fig. 9 and Figs. B.1 - B.3 shows thermospheric outputs for case ES; cases EH and EF are represented in columns two and three respectively.

For case ES, the zonal and meridional flows are very similar to those discussed in Yates et al. (2012) as the only difference between both steady-state compressed cases is that here we assume a constant height-integrated Pedersen conductivity whilst in Yates et al. (2012) the conductivity is enhanced by FAC. Zonally, there exists a small super-corotational jet at low altitudes in region III and a pair of large sub-corotational jets across regions II and I. The degree of sub-corotation is small compared with CS due to the highly compressed nature of the ES magnetosphere and the conservation of momentum. The meridional flows show a relatively large area of localised acceleration in regions II and I which, as explained above (section 3.2) and in Yates et al. (2012), is primarily due to the advection of momentum. Likewise, the direction of meridional flows is as discussed in section 3.2.

Thermospheric flows for case EH are slightly different from those of case ES. Zonally, there is a very small super-corotational jet (∼25 % that of CS) and the degree of sub-corotation has increased over the entire thermosphere as shown in Fig. 9b. This is caused by the large decrease in magnetospheric corotation accompanying the expansion (Fig. 2b). Large negative ion drag (three times larger than case ES, see Fig. B.1b) causes the thermosphere to lose a great amount of angular momentum (to magnetospheric plasma) which increases its degree of sub-corotation. In the meridional direction, in Fig. 9e, the low altitude accelerated poleward flow in regions II and I has increased in size and velocity (∼30 %) and there now exists another accelerated region of equatorward flow from mid to high altitudes centred at ∼73 °. Inspection of Fig. B.2k (meridional advection of momentum) shows areas of negative advection (red contours) at low altitudes of regions II and I which produce the poleward acceleration region. The positive advection contour (blue) located in the middle of region III and at altitudes above ∼450 km, creates the equatorward accelerated flow in this region. The direction of meridional flow indicated by the black arrows has also changed, mainly in region II, where flow at all altitudes is now directed poleward. Finally, in Fig. 9h, there is a significant increase in temperature (∼50 K) in region III and I, near the Pedersen conductivity layer, resulting from these dynamical changes. Paper 2 will discuss the corresponding changes in heating rates in more detail.

The thermospheric quantities at the end of the transient expansion event are shown in the third column of Fig. 9 and Figs. B.1- B.3. Considering Figs. 9c, f and i we see that the only change in zonal flow patterns is a slight increase in the zonal velocity. The meridional flows show a large poleward accelerated flow originating at low altitudes in region III and reaching the high altitudes of region I. Two smaller regions of accelerated equatorward flow arise in the upper altitudes of regions III and II. The temperature difference between cases EF and ES show increases in temperature up to $\sim$50 K co-located with accelerated meridional flow and decreases in temperature ($\sim$20 K) between these accelerated regions. As the magnetosphere returns to its initial compressed configuration, it weakly super-corotates over most of region III; this transfers angular momentum to the sub-corotating thermosphere which can essentially 'spin up' the latter. This effect can be seen in the zonal momentum terms shown in the third column of Fig. B.1 where the majority of momentum terms in regions III and II are positive and thus promote corotation. Fig. B.2l clearly shows that the large poleward accelerated region and temperature deviations result from the advection of meridional momentum (negative (red) contour) and its effect on heat transport (more detail in Paper 2).

Compared to the transient compression case CF, the EF thermosphere seems fairly stable i.e. there are no sharp peaks and troughs in the upper boundary. Our interpretation is that for the compression scenario the magnetosphere transfers a large amount of angular momentum to the thermosphere due to its large degree of super-corotation. This surge in momentum and energy input to the thermosphere over a short time scale causes significant strain on the thermosphere and thus requires a drastic reconfiguration in order to attempt to re-establish equilibrium. On the other hand, in our expansion scenario the magnetosphere significantly sub-corotates for most of the event and only super-corotates compared to the planet and thermosphere slightly nearing the end of the event. So for the majority of the transient event the thermosphere is losing angular momentum to the magnetosphere. Thus, its dynamics and energy input are generally smaller than the transient compression scenario. This leads to a less 'drastic' reaction. The influence of these transient events on heating in Jupiter's thermosphere will be discussed in our companion paper.

5. Discussion

We now discuss the steady-state, 'half-pulse' and 'full-pulse' results found in this study. As discussed in section 2.1 and 2.5, if we assume that the transient event occurs on small time scales ($\sim 2-3$ hours), plasma angular momentum is conserved. Therefore, the initial and final magnetospheric states will be identical (see Fig. 2).

In the compression scenario we observe super-corotation of the middle magnetosphere with angular velocities up to $\sim 1.6\,\Omega_J$. This changes both the dynamics and M-I current systems in the thermosphere and magnetosphere. Thermospheric angular velocities are positively correlated to what happens in the magnetosphere, so with magnetospheric super-corotation the thermosphere responds by increasing its angular velocity. The response is, however, not as strong as that of the magnetosphere due to the immense inertia of the thermosphere. Thus, its response lags behind the magnetospheric response in region III; regions II and I show a small response. With regards to the coupling currents, the initial and final states show little variability, depending mainly on contributions from the lagging thermosphere. Midway through the pulse, there is a current reversal (see Figs. 3-4). This reversal is caused by the super-corotation of the magnetosphere and indicates that angular momentum is now being transferred from magnetosphere to thermosphere, contrary to steady state momentum transfer. This deposits energy and 'spins up' the thermosphere and planet (Cowley et al., 2007). We expect a significant auroral response to a transient compression; FAC densities (Fig. 4) suggest that the main auroral oval's brightness would double and shift polewards by $\sim 0.2^\circ$ (Nichols et al., 2009; Clarke et al., 2009). We would also expect noticeable auroral activity around the open-closed (region II/I) boundary (although this effect is sensitive to the plasma flow models used in these regions).

The thermospheric response to this transient compression event is more complicated than that of the magnetosphere (see Figs. 6 and A.1 - A.3). Initially, the thermosphere is in a steady-state and momentum terms are balanced (see section 3.2, Yates et al. (2012) and Smith and Aylward (2009) for more detail on steady state flows). Midway through the event, significant dynamic changes occur in the thermosphere and it can no longer be considered to be in dynamic equilibrium. Zonal and meridional velocities increase due to reversals in the direction of ion drag. At the end of the event, thermospheric velocities have increased further and there are now many meridionally accelerated regions. Ion drag, Coriolis and advection momentum terms create the complex accelerated flow systems most pronounced in the meridional flows. This leads to temperature changes $>25\,K$ in the highly accelerated regions and distorts the high altitude thermosphere. Such temperature changes may be observationally detectable, through infrared spectroscopic techniques (Stallard et al., 2002).

Considering the transient expansion scenario, we find that the degree of corotation of plasma angular velocity significantly decreases midway through the expansion event (maximum expansion). This causes a reduction in thermospheric angular velocity. These combined changes result in a large flow shear between the thermosphere and magnetosphere which correspondingly increases the magnitude of M-I coupling currents (see Figs. 7-8). The FAC profiles midway through the event indicate little increase in auroral brightness ($\sim$15 %) and an equatorward shift in peak emission of $\sim 1^\circ$. FAC profiles also indicate main oval broadening of $\sim 2^\circ$ and the disappearance of polar emission. Thus, the auroral response for a transient expansion is less pronounced than that of a compression of similar magnitude (Clarke et al., 2009). At the end of the event, the magnetosphere super-corotates compared to the thermosphere, indicating the lag in thermospheric response time resulting from its large inertia. This creates a small amount of current reversal which acts to ‘spin up’ the thermosphere.

The initial thermospheric flows for our expansion scenario (compressed steady-state) are discussed in section 4.2, Yates et al. (2012) and Smith and Aylward (2009). Midway through the event, the main changes in zonal and meridional momentum balance occur in ion drag and advection terms. These changes decrease the degree of corotation and reverse high altitude meridional flow patterns. Upon completion of the event, thermospheric velocities are increased due to the ”newly” compressed nature of the magnetosphere. Poleward accelerated flows encompass most of the upper latitudes ($>74^\circ$). These accelerated flows efficiently transport energy across the thermosphere and lead to temperature variations of >40 K.

6. Conclusion

We have investigated the effect of transient variations in solar wind dynamic pressure on the M-I coupling currents and thermospheric flows of the Jovian system. In this paper, we concentrate mainly on the response of thermospheric dynamics to these transient variations in the solar wind. We considered two scenarios: i) a transient compression event, and ii) a transient expansion event. Both of these were imposed over a time scale of three hours. A transient compression event consists of an initially expanded, steady-state magnetospheric configuration. The model Jovian magnetosphere then encounters a shock in the solar wind, which compresses the system. As the conceptual shock traverses past the magnetosphere, a rarefaction region follows and the magnetosphere subsequently expands back to its initial state. The opposite occurs for our expansion event. In sections 3 and 4 we presented the modelled response of M-I coupling currents and thermospheric flows to these events.

To summarise, the response of the magnetosphere to transient variations in solar wind dynamic pressure is similar to predictions and modelling by Cowley and Bunce (2003a,b) and Cowley et al. (2007). Transient compressions cause the magnetosphere to super-corotate compared to both planet and thermosphere. This results in the reversal of coupling currents and angular momentum transfer which 'spin up' the planet and deposit energy in the thermosphere. The main auroral oval is shifted polewards ($\sim 0.2\,^{\circ}$) and its brightness is doubled; our modelling also suggest emission in the outer magnetosphere and polar cap. Transient expansions, on the other hand, cause a significant increase in the degree of sub-corotation which increases the flow shear between the magnetosphere and thermosphere and leads to increases in coupling currents. There is an increase in angular momentum transfer from the thermosphere to magnetosphere, which acts to accelerate the magnetospheric plasma towards corotation. Thus, the thermosphere loses energy and angular momentum. We predict a $\sim 2\,^{\circ}$ broadening of the main oval and an equatorward shift of $\sim 1\,^{\circ}$ in peak emission, as well as a reduction in polar emission. The modelled auroral responses are supported by observation studies by Nichols et al. (2009) and Clarke et al. (2009).

To our knowledge, this is the first study that considers the response of the Jovian thermosphere to variations in solar wind pressure on relatively short time scales. The most significant changes to the thermosphere occurred at the end of the transient event. We found a positive correlation between the thermospheric and magnetospheric angular velocities. However, the thermospheric response lags behind that of the magnetosphere due to its large inertia. Dynamically, the most pronounced changes in the thermosphere occurred in ion drag and advection terms. The latter created large accelerated meridional flows which subsequently increased and decreased the thermospheric temperature, particularly in regions mapping to the middle and outer magnetosphere. Previous studies have found that the thermosphere reacts immediately ($\sim$30 minutes) to magnetospheric changes (Millward et al., 2005) or have assumed no reaction at all (Gong, 2005). Overall, we find that our model's thermospheric response lies in between these limits, but is more similar to the 'non-responsive' case. In other words, the thermosphere does respond to the imposed magnetospheric changes, but with a considerable 'lag' in time, comparable to or longer than the timescale ($\sim$3 hours) of that imposed change.

Acknowledgement

JNY was supported by an STFC studentship award. The authors acknowledge support of the STFC funded Miracle Consortium (part of the DiRAC facility) in providing access to computational resources. The authors express their gratitude to Chris Smith who developed the GCM used herein.

References

Achilleos, N., Miller, S., Tennyson, J., Aylward, A. D., Mueller-Wodarg, I., Rees, D., 1998. JIM: A time-dependent, three-dimensional model of Jupiter's thermosphere and ionosphere. J. Geophys. Res. 103, 20089–20112.

Clarke, J. T., Nichols, J., Gérard, J.-C., Grodent, D., Hansen, K. C., Kurth, W., Gladstone, G. R., Duval, J., Wannawichian, S., Bunce, E., Cowley, S. W. H., Crary, F., Dougherty, M., Lamy, L., Mitchell, D., Pryor, W., Retherford, K., Stallard, T., Zieger, B., Zarka, P., Cecconi, B., May 2009. Response of Jupiter's and Saturn's auroral activity to the solar wind. Journal of Geophysical Research (Space Physics) 114, 5210.

Connerney, J. E. P., Acuña, M. H., Ness, N. F., Satoh, T., 1998. New models of Jupiter's magnetic field constrained by the Io flux tube footprint. J. Geophys. Res. 103, 11929–11940.

Connerney, J. E. P., Acuna, M. H., Ness, N. F., 1981. Modeling the Jovian current sheet and inner magnetosphere. J. Geophys. Res. 86, 8370–8384.

Cowley, S. W. H., Alexeev, I. I., Belenkaya, E. S., Bunce, E. J., Cottis, C. E., Kalegaev, V. V., Nichols, J. D., Prangé, R., Wilson, F. J., 2005. A simple axisymmetric model of magnetosphere-ionosphere coupling currents in Jupiter's polar ionosphere. J. Geophys. Res. 110, 11209–11226.

Cowley, S. W. H., Bunce, E. J., 2003a. Modulation of Jovian middle magnetosphere currents and auroral precipitation by solar wind-induced compressions and expansions of the magnetosphere: initial response and steady state. Planet. Space Sci. 51, 31–56.

Cowley, S. W. H., Bunce, E. J., 2003b. Modulation of Jupiter's main auroral oval emissions by solar wind induced expansions and compressions of the magnetosphere. Planet. Space Sci. 51, 57–79.

Cowley, S. W. H., Nichols, J. D., Andrews, D. J., 2007. Modulation of Jupiter's plasma flow, polar currents, and auroral precipitation by solar wind-induced compressions and expansions of the magnetosphere: a simple theoretical model. Ann. Geophys. 25, 1433–1463.

Gong, B., 2005. Variations of Jovian aurora induced by changes in solar wind dynamic pressure. Ph.D. thesis, Rice University.

Hill, T. W., 1979. Inertial limit on corotation. J. Geophys. Res. 84, 6554–6558.

Huang, T. S., Hill, T. W., 1989. Corotation lag of the Jovian atmosphere, ionosphere, and magnetosphere. J. Geophys. Res. 94, 3761–3765.

Isbell, J., Dessler, A. J., Waite, Jr., J. H., 1984. Magnetospheric energization by interaction between planetary spin and the solar wind. J. Geophys. Res. 89, 10716–10722.

Joy, S. P., Kivelson, M. G., Walker, R. J., Khurana, K. K., Russell, C. T., Ogino, T., 2002. Probabilistic models of the Jovian magnetopause and bow shock locations. J. Geophys. Res. 107, 1309–1325.

Khurana, K. K., Kivelson, M. G., 1993. Inference of the angular velocity of plasma in the Jovian magnetosphere from the sweepback of magnetic field. J. Geophys. Res. 98, 67–79.

Millward, G., Miller, S., Stallard, T., Achilleos, N., Aylward, A. D., Jan. 2005. On the dynamics of the jovian ionosphere and thermosphere. Icarus 173, 200–211.

Müller-Wodarg, I. C. F., Mendillo, M., Yelle, R. V., Aylward, A. D., Jan. 2006. A global circulation model of Saturn's thermosphere. Planet. Space Sci.180, 147–160.

Nichols, J., Cowley, S., 2004. Magnetosphere-ionosphere coupling currents in Jupiter's middle magnetosphere: effect of precipitation-induced enhancement of the ionospheric Pedersen conductivity. Ann. Geophys. 22, 1799–1827.

Nichols, J. D., Clarke, J. T., Gérard, J. C., Grodent, D., Hansen, K. C., Jun. 2009. Variation of different components of Jupiter's auroral emission. Journal of Geophysical Research (Space Physics) 114, 6210.

Pontius, D. H., 1997. Radial mass transport and rotational dynamics. J. Geophys. Res. 102, 7137–7150.

Ray, L. C., Ergun, R. E., Delamere, P. A., Bagenal, F., Sep. 2010. Magnetosphere-ionosphere coupling at Jupiter: Effect of field-aligned potentials on angular momentum transport. Journal of Geophysical Research (Space Physics) 115, 9211.

Ray, L. C., Ergun, R. E., Delamere, P. A., Bagenal, F., Jan. 2012. Magnetosphere-ionosphere coupling at Jupiter: A parameter space study. Journal of Geophysical Research (Space Physics) 117, 1205.

Smith, C. G. A., Aylward, A. D., 2008. Coupled rotational dynamics of Saturn's thermosphere and magnetosphere: a thermospheric modelling study. Ann. Geophys. 26, 1007–1027.

Smith, C. G. A., Aylward, A. D., 2009. Coupled rotational dynamics of Jupiter's thermosphere and magnetosphere. Ann. Geophys. 27, 199–230.

Smith, C. G. A., Aylward, A. D., Millward, G. H., Miller, S., Moore, L. E., 2007. An unexpected cooling effect in Saturn's upper atmosphere. Nature 445, 399–401.

Southwood, D. J., Kivelson, M. G., 2001. A new perspective concerning the influence of the solar wind on the Jovian magnetosphere. J. Geophys. Res. 106, 6123–6130.

Stallard, T., Miller, S., Millward, G., Joseph, R. D., Apr. 2002. On the Dynamics of the Jovian Ionosphere and Thermosphere. II. The Measurement of $H_3{}^+$ Vibrational Temperature, Column Density, and Total Emission. Icarus 156, 498–514.

Tao, C., Fujiwara, H., Kasaba, Y., 2009. Neutral wind control of the Jovian magnetosphere-ionosphere current system. J. Geophys. Res. 114, 8307–8323.

Yates, J., Achilleos, N., Guio, P., 2012. Influence of upstream solar wind on thermospheric flows at jupiter. Planetary and Space Science 61 (1), 15 – 31, surfaces, atmospheres and magnetospheres of the outer planets and their satellites and ring systems: Part VII.

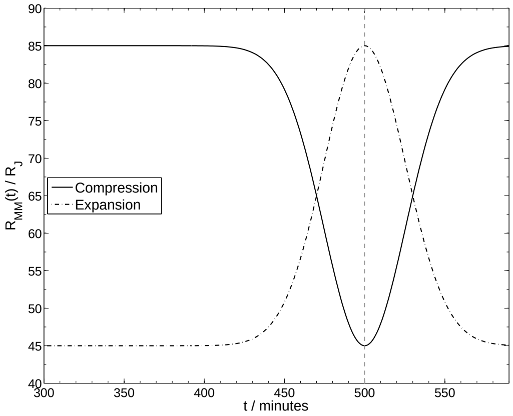

Figure 1: The variation of magnetodisc radius $R_{MM}(t)$ with time during a pulse in the solar wind. The black solid and dot-dashed lines represent a compression and expansion respectively throughout the entire pulse. The grey dashed line indicates the point of maximum variation.

Appendix A. Compression event momentum terms

Figs. A.1 - A.3 show contour maps for ion drag, Coriolis, advection, viscous and pressure gradient thermospheric acceleration terms. Contours are plotted on latitude and altitude Pedersen conductivity distributions (indicated on the colour bar). Positive acceleration terms are represented by blue contours whilst negative terms are represented by red contours. These figures are used to aid in the interpretation of thermospheric flows in section 3.2 (Fig. 6). More specifically, Fig. A.1 shows zonal acceleration terms whilst Figs. A.2 - A.3 show meridional acceleration terms.

Appendix B. Expansion event momentum terms

Figs. B.1 - B.3 show contour maps for ion drag, Coriolis, advection, viscous and pressure gradient thermospheric acceleration terms. Contours are plotted on latitude and altitude Pedersen conductivity distributions (indicated on the colour bar). Positive acceleration terms are represented by blue contours whilst negative terms are represented by red contours. These figures are used to aid in the interpretation of thermospheric flows in section 4.2 (Fig. 9). More specifically, Fig. B.1 shows zonal acceleration terms whilst Figs. B.2 - B.3 show meridional acceleration terms.

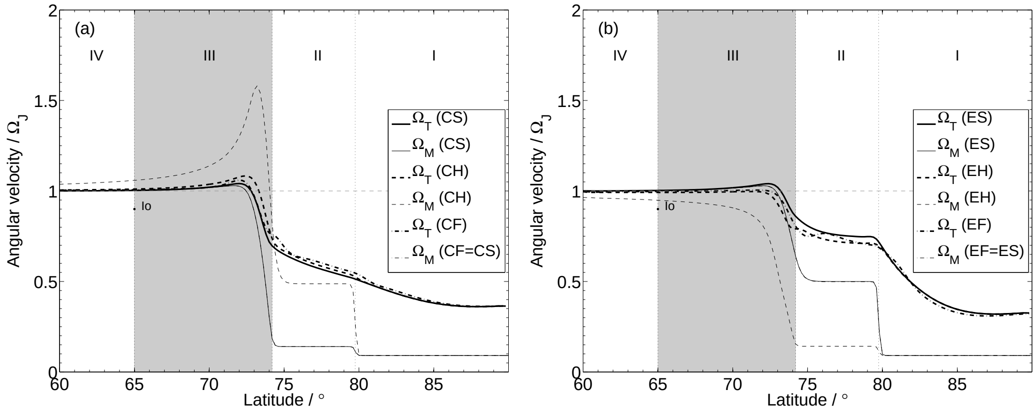

Figure 2: (a) Thermospheric and plasma angular velocity profiles for the transient compression cases as a function of ionospheric latitude. Thick lines represent thermospheric profiles whilst thin lines represent plasma profiles. The solid lines represent case CS (steady state before compression) whilst the dashed and dot-dashed lines indicate cases CH (system at minimum disc radius) and CF (system just returned to initial disc radius) respectively. The magnetospheric regions (region III shaded) are labelled and separated by the black dotted lines. The magnetically mapped location of Io on the ionosphere is marked and labelled. (b) Thermosphere and plasma angular velocity profiles for the transient expansion cases as a function of ionospheric latitude. The line styles are the same as (a) but the cases are now ES, EH and EF respectively, where 'E' denotes expansion, and the 'S', 'H' and 'F' symbols represent the same phases of the event as for Fig. 2a.

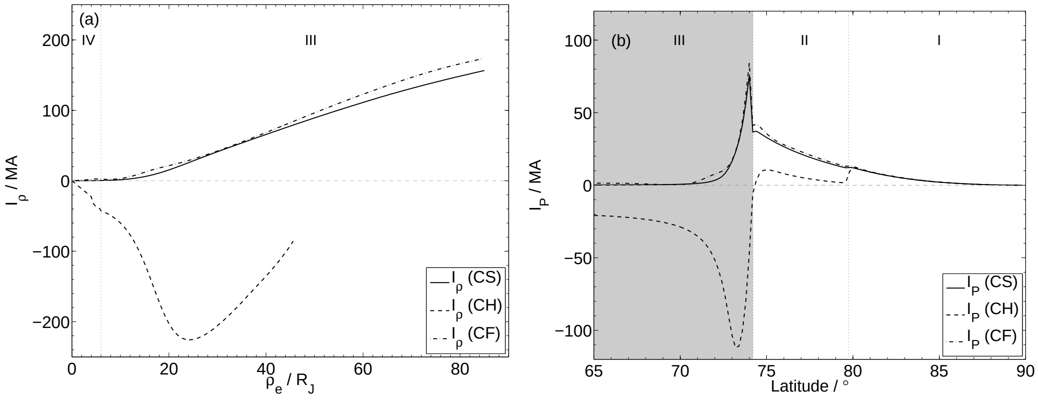

Figure 3: (a) Azimuthally integrated radial current as a function of equatorial radial distance from Jupiter. The solid line represents case CS, whilst the dashed and dot-dashed lines indicate cases CH and CF, respectively. (b) Azimuthally integrated Pedersen current as a function of ionospheric latitude. The line styles are the same as in (a). The dotted black lines separate the magnetospheric regions considered in this study. Positive I_P indicates equatorward current.

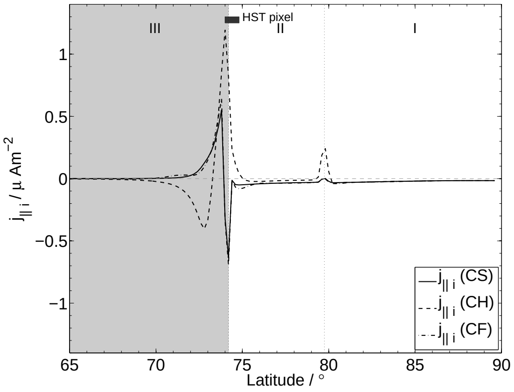

Figure 4: FAC densities in the high latitude ionospheric region for our transient compression cases. The solid line represents case CS whilst the dashed and dot-dashed lines indicate cases CH and CF respectively. The conjugate magnetospheric regions (region III is shaded) are separated by dotted black lines and labelled. The latitudinal size of an ACS-SBC HST pixel located near the main auroral emission is represented by the dark grey box.

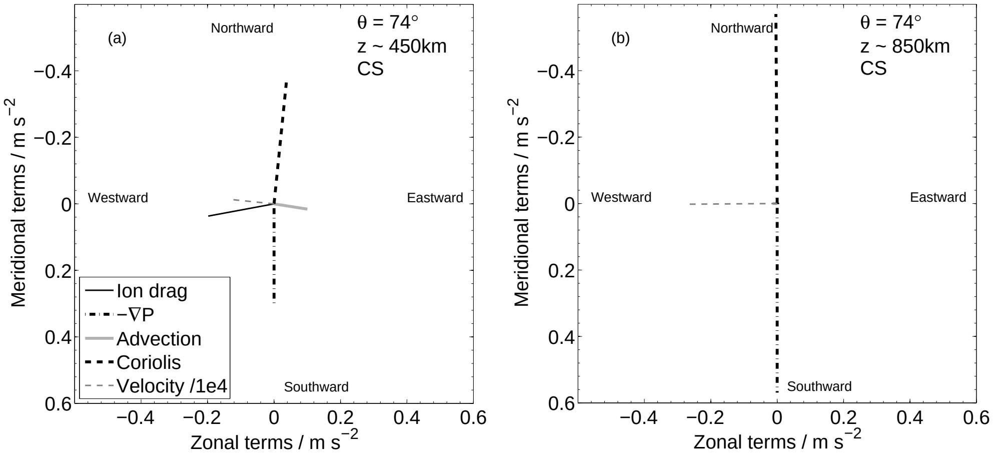

Figure 5: Meridional and zonal acceleration balance diagrams for case CS at an ionospheric latitude of 74 °. (a) Shows acceleration terms at low altitude whilst (b) shows the equivalent terms at high altitude. Ion drag terms are represented by thin black solid lines, fictitious (Coriolis) by thick black dashed lines, pressure gradient by thick black dot-dashed lines and advection by the thin grey solid lines. The velocity vector (in the corotating reference frame) is represented by the thin grey dashed lines. Note that the magnitude of velocity components have been divided by a factor of $10,000$ to fit the plotted scale.

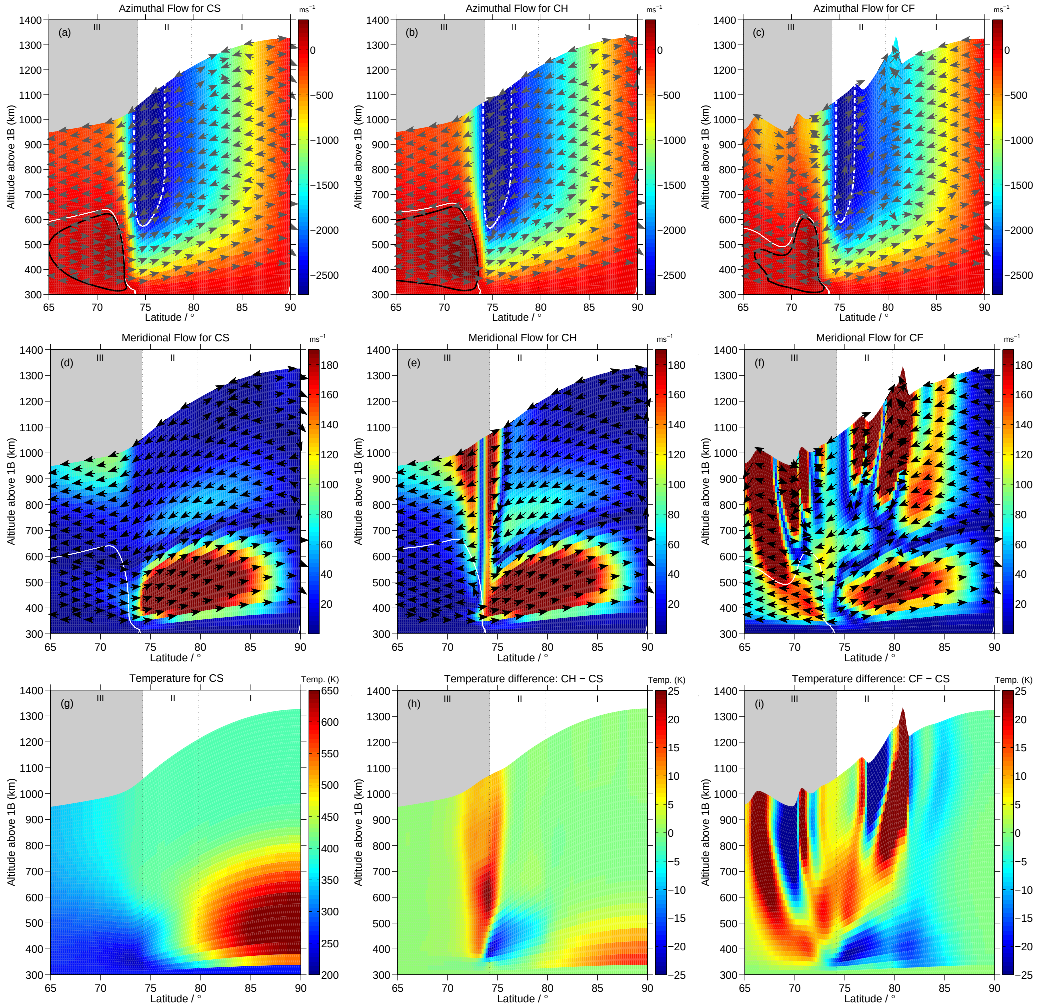

Figure 6: (a)-(c) show the variation of thermospheric azimuthal velocity (colour scale) in the corotating reference frame for cases CS-CF respectively (left to right). Positive values (dark red) indicate super-corotation, whilst negative values (light red to blue) indicate sub-corotation. The arrows show the direction of meridional flow and the solid white line indicates the locus of rigid corotation. The solid black encloses regions of super-corotation ($> 25\,\mathrm{m\,s^{-1}}$) and the dashed white line encloses regions that are sub-corotating at a rate $> -2500\,\mathrm{m\,s^{-1}}$. The magnetospheric regions (region III is shaded) are separated by dotted black lines and labelled. (d)-(f) show the meridional velocity in the thermosphere for cases CS-CF. The colour scale indicates the speed of flows. All other labels and are as for (a)-(c). (g) shows the thermospheric temperature distributions for case CS whilst (h)-(i) show the temperature difference of cases CH and CF with case CS. All labels are as in (a)-(c).

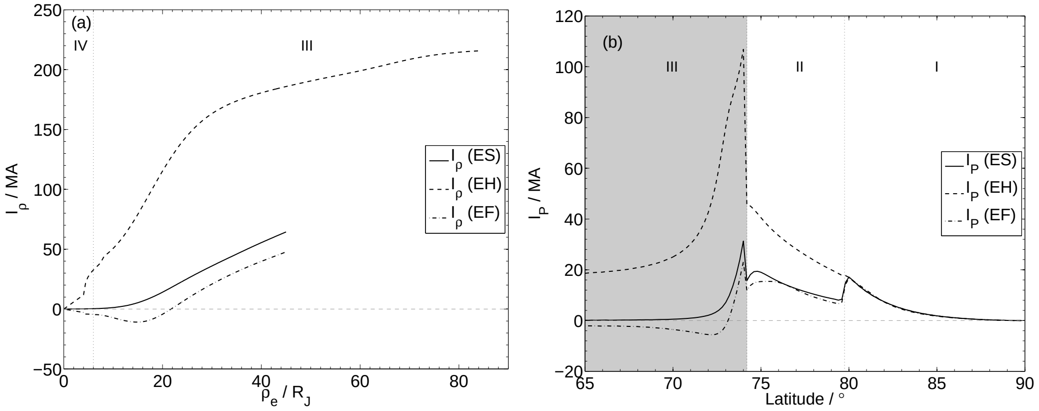

Figure 7: (a) Azimuthally integrated radial current as a function of equatorial radial distance from Jupiter. The solid line represents case ES whilst the dashed and dot-dashed lines indicate cases EH and EF respectively. (b) Azimuthally integrated Pedersen current as a function of ionospheric latitude. The line style code is the same as in (a) whilst the dotted black lines separate the magnetospheric regions considered in this study (region III is shaded).

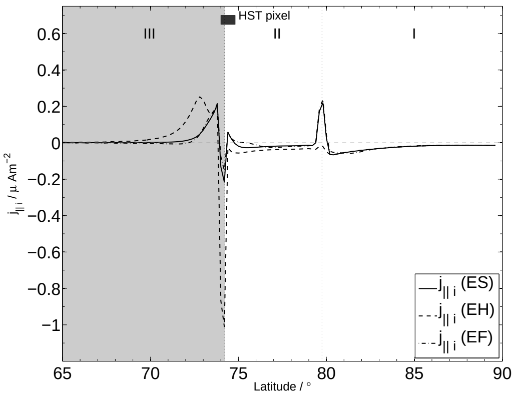

Figure 8: FAC densities in the high latitude region for our transient expansion cases. The solid line represents case ES whilst the dashed and dot-dashed lines indicate cases EH and EF respectively. The magnetospheric regions (region III is shaded) are separated by dotted black lines and labelled. The latitudinal size of an ACS-SBC HST pixel is indicated by the dark grey box.

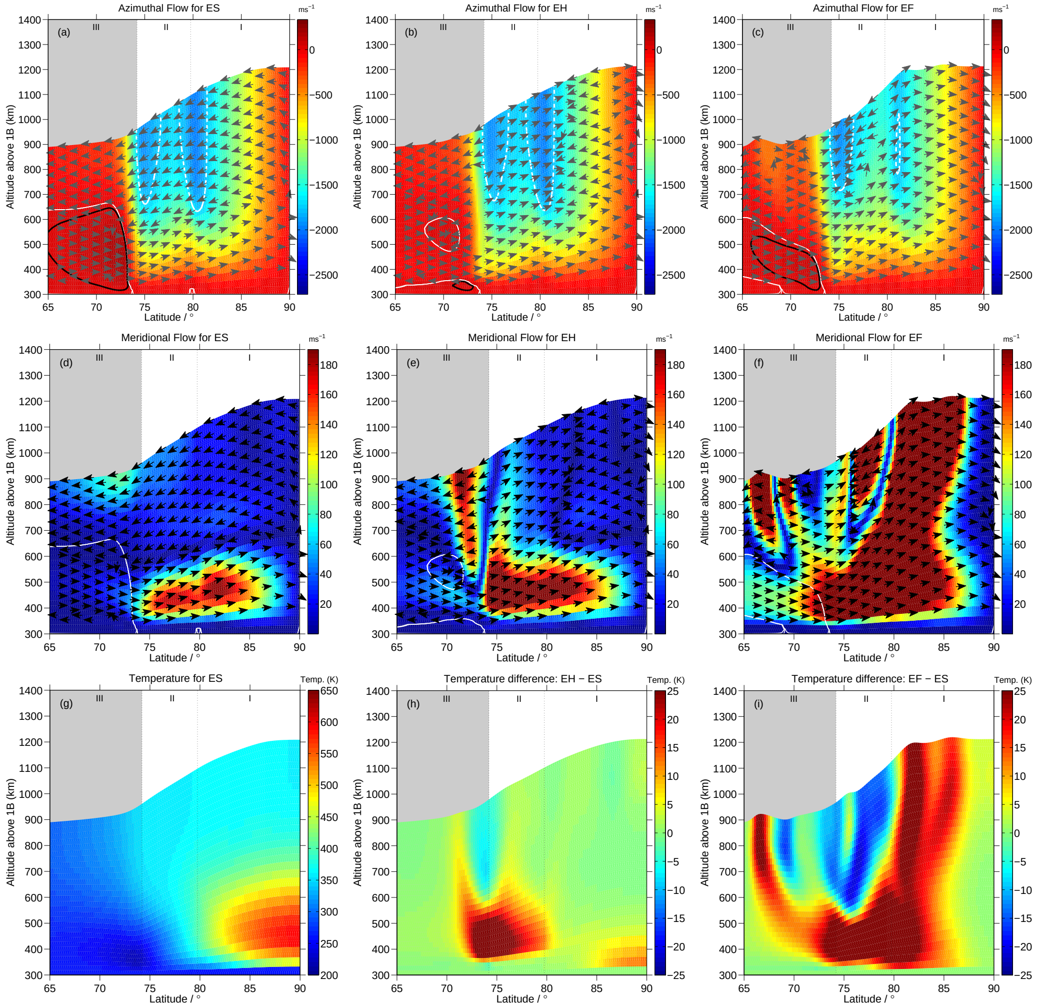

Figure 9: (a)-(c) show the variation of thermospheric azimuthal velocity (colour scale) in the corotating reference frame for cases ES-EF respectively (left to right). Positive values (dark red) indicate super-corotation, whilst negative values (light red to blue) indicate sub-corotation. The arrows show the direction of meridional flow and the white line indicates the locus of rigid corotation. The solid black encloses regions of super-corotation ($> 25\,\mathrm{m\,s^{-1}}$) and the dashed white line encloses regions that are sub-corotating at a rate $> -1750\,\mathrm{m\,s^{-1}}$. The magnetospheric regions (region III is shaded) are separated by dotted black lines and labelled. (d)-(f) show the meridional velocity in the thermosphere for cases ES-EF. The colour scale indicates the speed of flows. All other labels and are as for (a)-(c). (g) shows the thermospheric temperature distributions for case ES whilst (h)-(i) show the temperature difference between cases EH and EF and case ES. All labels are as in (a)-(c).

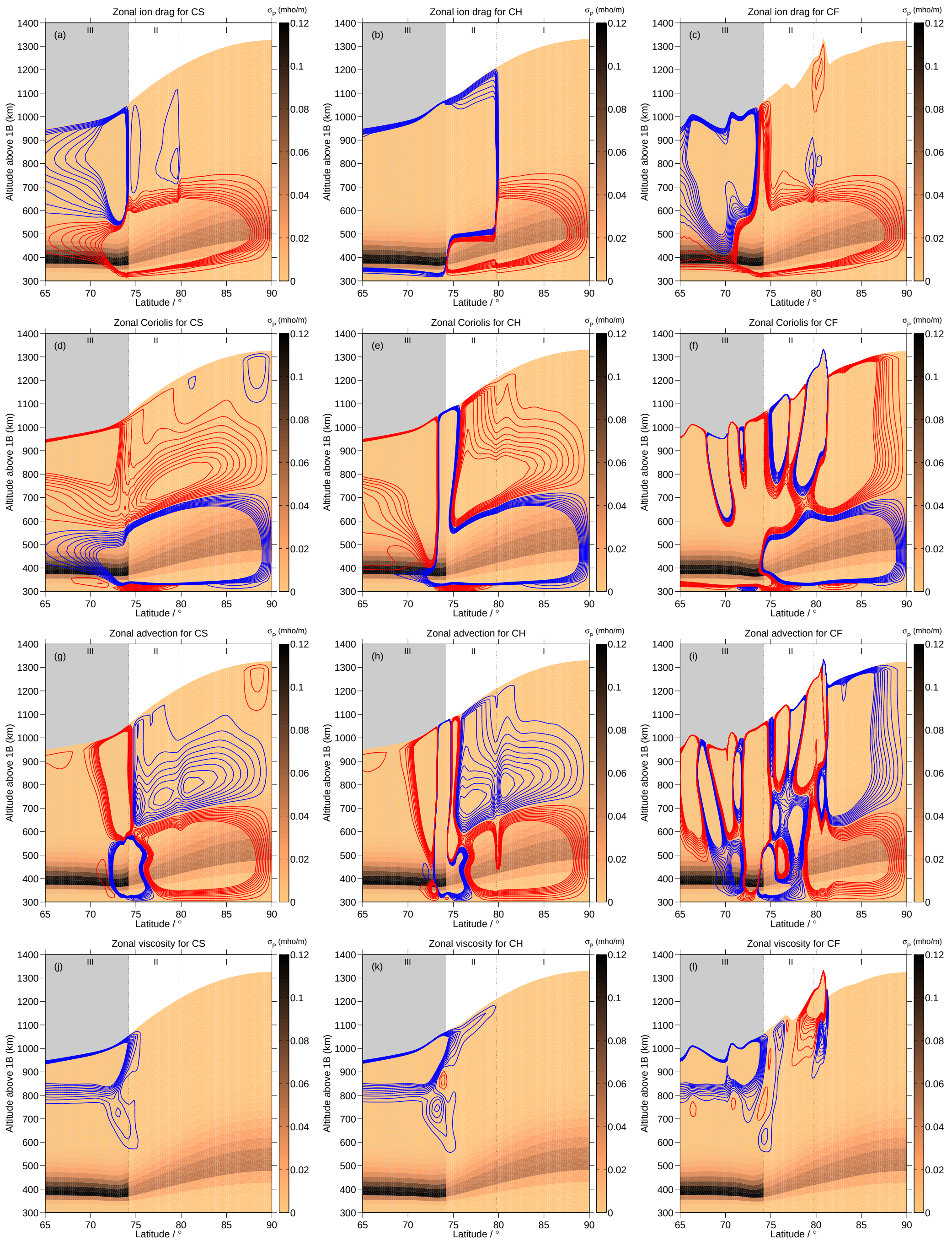

Figure A.1: (a)-(c) shows the variation of zonal ion drag momentum with altitude, latitude and Pedersen conductance (colour bar) for cases CS, CH and CF (left to right). The contours range from $1 - 10\,\mathrm{mm\,s^{-2}}$ with an interval of $1\,\mathrm{mm\,s^{-2}}$ but with blue being positive and red negative. The magnetospheric regions are separated and labelled. (d)-(l) represent zonal momentum terms related to Coriolis, advection and viscosity respectively. All colours and labels are as in (a)-(c).

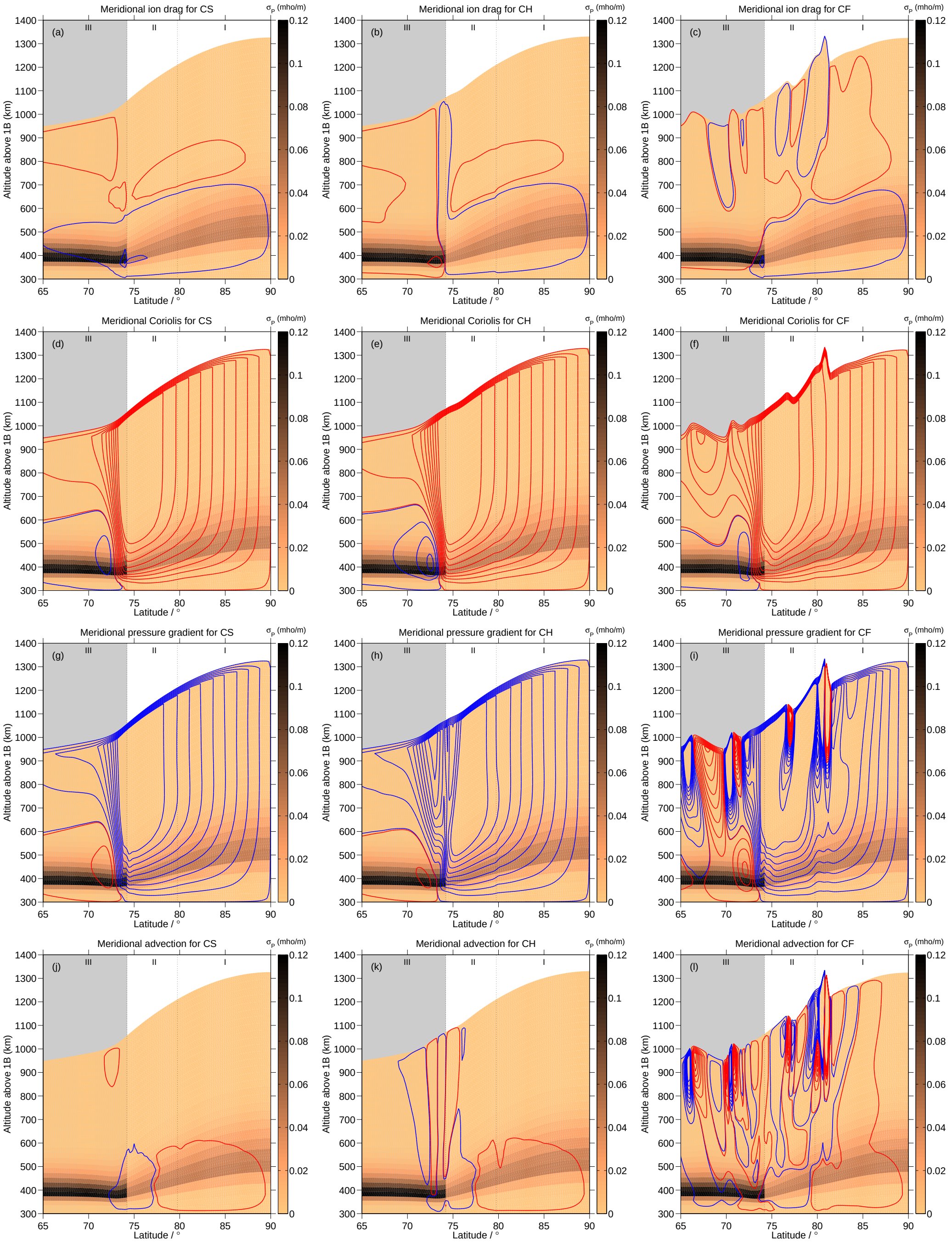

Figure A.2: (a)-(c) shows the variation of meridional ion drag momentum with altitude, latitude and Pedersen conductance (colour bar) for cases CS, CH and CF (left to right). The contours range from $1 - 500\,\mathrm{mm\,s^{-2}}$ with an interval of $50\,\mathrm{mm\,s^{-2}}$ but with blue being positive and red negative. The magnetospheric regions are separated and labelled. (d)-(l) represent meridional momentum terms related to Coriolis, pressure gradients and advection respectively. All colours and labels are as in (a)-(c).

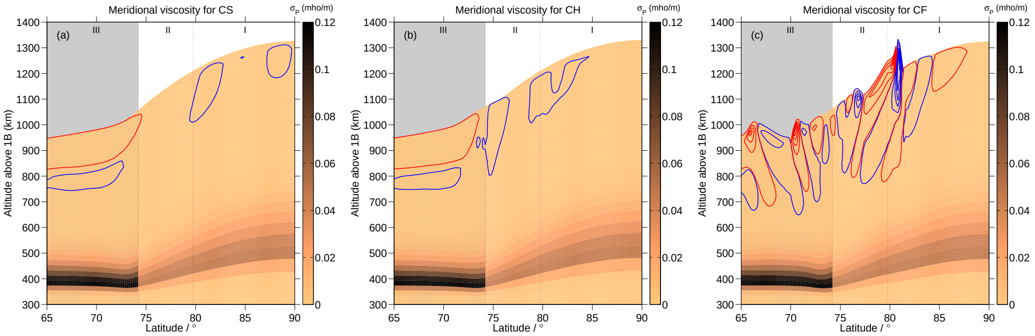

Figure A.3: (a)-(c) shows the variation of meridional viscosity with altitude, latitude and Pedersen conductance (colour bar) for cases CS, CH and CF (left to right). The contours range from $1 - 500\,\mathrm{mm\,s^{-2}}$ with an interval of $50\,\mathrm{mm\,s^{-2}}$ but with blue being positive and red negative. The magnetospheric regions are separated and labelled.

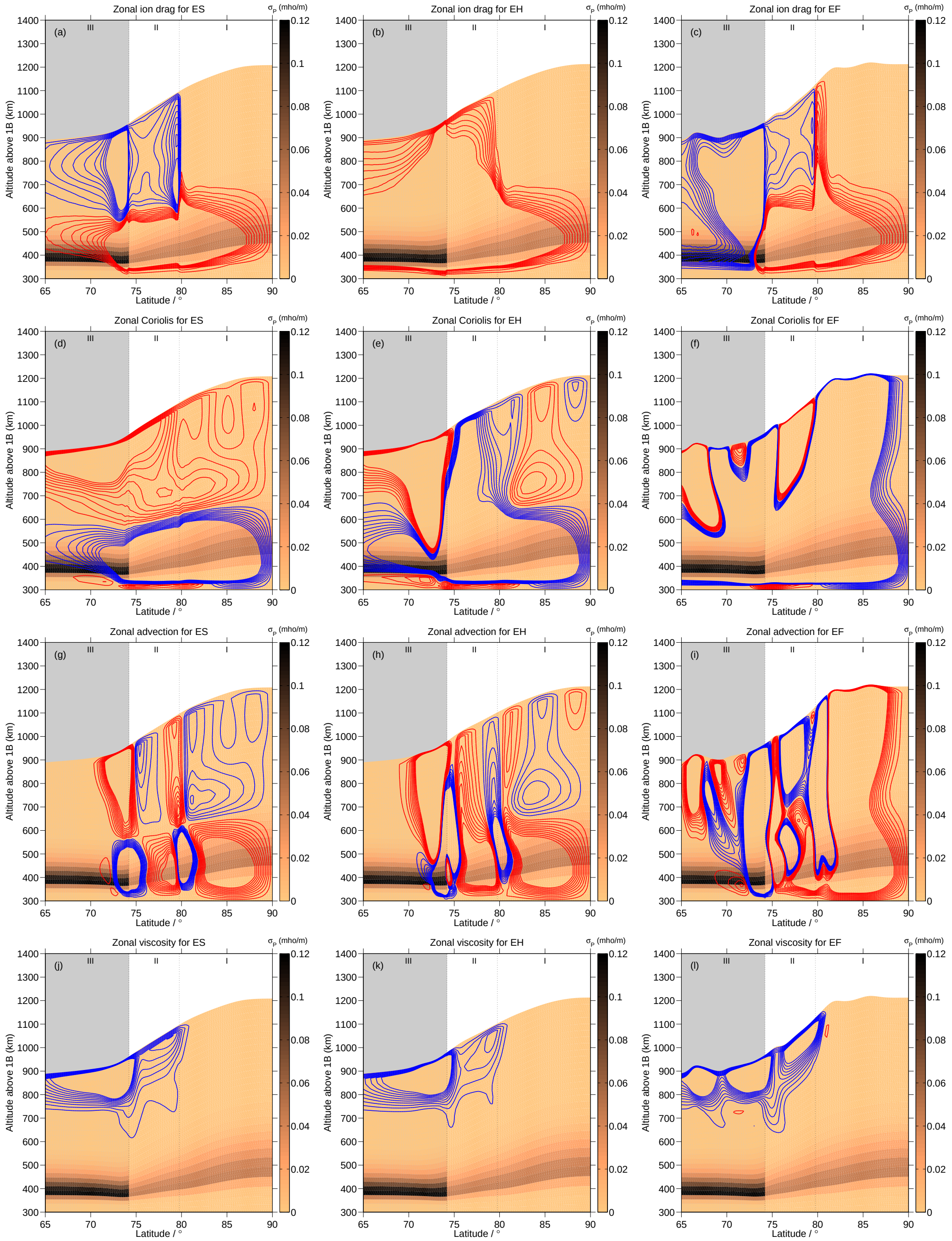

Figure B.1: (a)-(c) shows the variation of zonal ion drag momentum with altitude, latitude and Pedersen conductance (colour bar) for cases ES, EH and EF (left to right). The contours range from $1 - 10\,\mathrm{mm\,s^{-2}}$ with an interval of $1\,\mathrm{mm\,s^{-2}}$ but with blue being positive and red negative. The magnetospheric regions are separated and labelled. (d)-(l) represent zonal momentum terms related to Coriolis, advection and viscosity respectively. All colours and labels are as in (a)-(c).

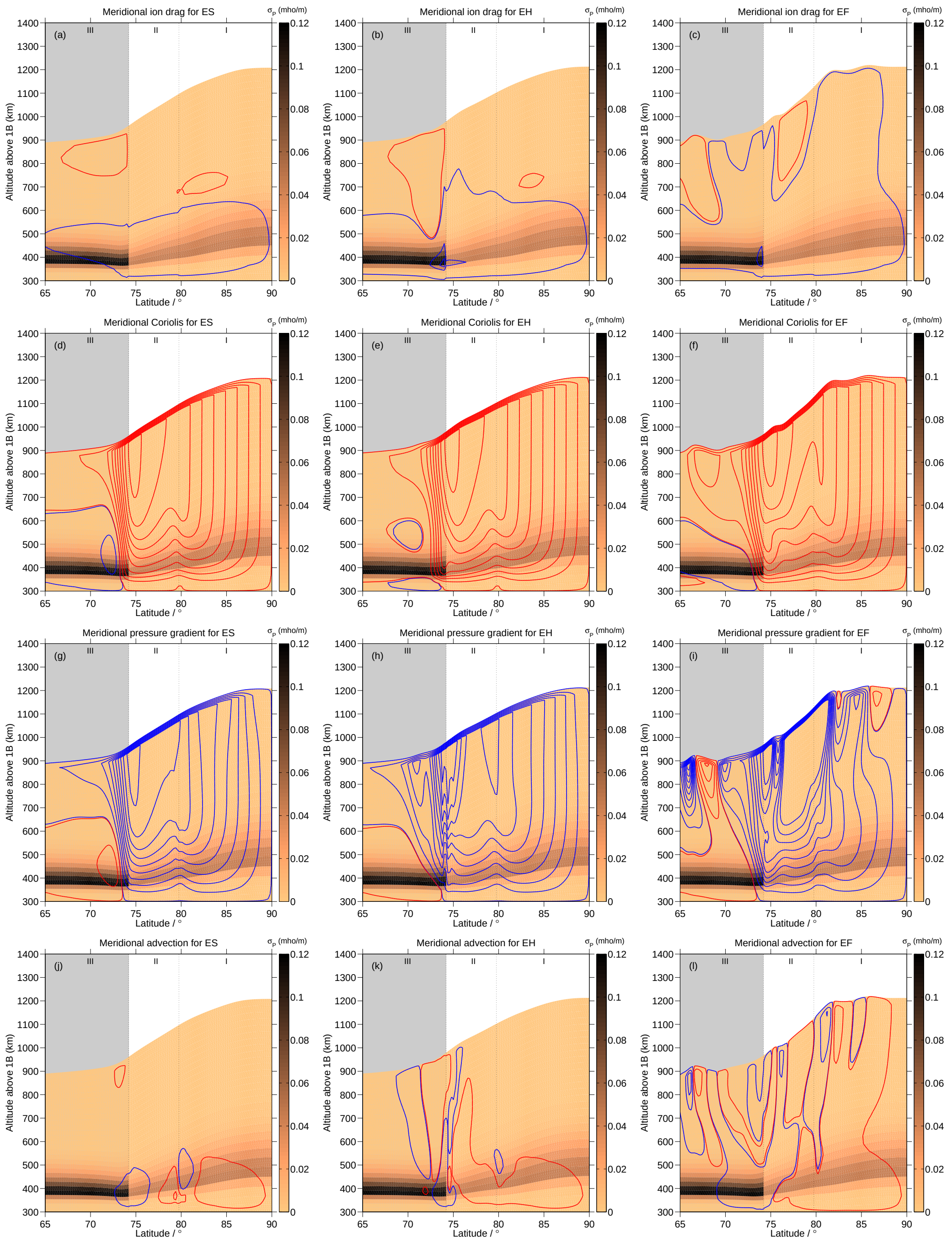

Figure B.2: (a)-(c) shows the variation of meridional ion drag momentum with altitude, latitude and Pedersen conductance (colour bar) for cases ES, EH and EF (left to right). The contours range from $1 - 500\,\mathrm{mm\,s^{-2}}$ with an interval of $50\,\mathrm{mm\,s^{-2}}$ but with blue being positive and red negative. The magnetospheric regions are separated and labelled. (d)-(l) represent meridional momentum terms related to Coriolis, pressure gradients and advection respectively. All colours and labels are as in (a)-(c).

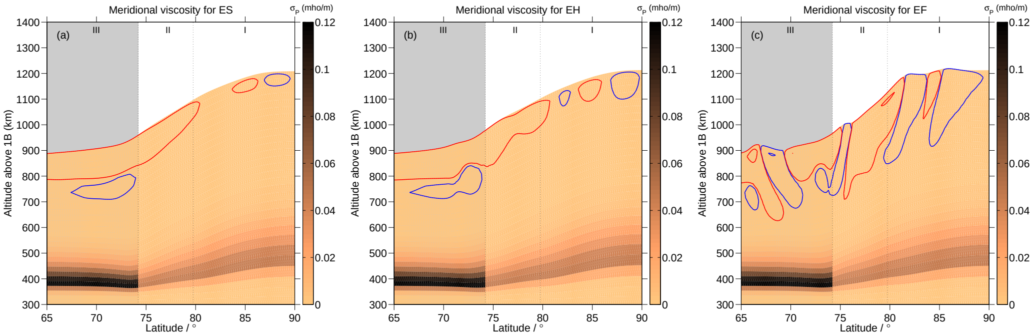

Figure B.3: (a)-(c) shows the variation of meridional viscosity with altitude, latitude and Pedersen conductance (colour bar) for cases ES, EH and EF (left to right). The contours range from $1 - 500\,\mathrm{mm\,s^{-2}}$ with an interval of $50\,\mathrm{mm\,s^{-2}}$ but with blue being positive and red negative. The magnetospheric regions are separated and labelled.